



DELIVERABLE

Project Acronym	BioMembrOS
Project Title	Biomimetic Membranes for Organ Support
Project number	101130006
Call	HORIZON-EIC-2023-PATHFINDEROPEN-01
Topic	HORIZON-EIC-2023-PATHFINDEROPEN-01-01
Type of Action	HORIZON-EIC
Service	EISMEA/E/01
Project start date	January 1 st , 2024
Project duration	42 months

D3.1 Fiber Design Model

Work package	3
Due date	30.09.2024
Submission date	30.09.2024
Lead beneficiary for this deliverable	TUW

Dissemination level		
PU	Public – fully open	Х
SEN	limited under the conditions of the Grant Agreement	
EU Classified	RESTREINT-UE/EU-RESTRICTED, CONFIDENTIEL-UE/EU-CONFIDENTIAL, SECRET-UE/EU-SECRET under Decision 2015/444	



Revision chart

Revision	Date	Author	Beneficiary	Description
First draft	16.09.2024	Seyyed Hossein Monsefi	TUW	Complete draft
Second draft	23.09.2024	Seyyed Hossein Monsefi	TUW	Complete draft
Third draft	24.09.2024	Seyyed Hossein Monsefi Margit Gföhler	TUW	Complete draft
Fourth draft	24.09.2024	Seyyed Hossein Monsefi	TUW	Complete draft
Revision 1	29.09.2024	Giuseppina Montante, Cristiana Boi	UNIBO	
Final draft	30.09.2024	Seyyed Hossein Monsefi	TUW	Complete draft

Disclaimer: The information in this document is subject to change without notice. Company or product names mentioned in this document may be trademarks or registered trademarks of their respective companies.

All rights reserved.

The document is proprietary of the BioMembrOS consortium members. No copying or distributing, in any form or by any means, is allowed without the prior written agreement of the owner of the property rights.

This document reflects only the authors' view. The European Community is not liable for any use that may be made of the information contained herein.





This project has received funding from the European Union's Horizon Europe research and innovation programme under grant agreement Nº 101130006. Views and opinions expressed are however those of the author(s) only and do not necessarily reflect those of the European Union or European Innovation Council. Neither the European Union nor the granting authority can be held responsible for them.

CONTENTS

1	L EXECUTIVE SUMMARY	4
2	2 KEYWORD LIST	5
3	B LIST OF ACRONYMS	6
4	INTRODUCTION	8
5	METHODOLOGY	9
	5.1 CFD Domain	9
	5.2 Fluid Physical Properties and Investigated Conditions	
	5.3 GOVERNING EQUATIONS AND BOUNDARY CONDITIONS	13
	5.3.1 Boundary Condition Study	15
	5.4 Mesh Dependence Study	21
6	RESULTS AND DISCUSSION	24
	6.1 SINGLE FIBER	25
	6.1.1 Transverse Flow	25
	6.1.2 Parallel Flow	28
	6.2 Multi-fibers (20 Fibers)	32
	6.3 Multi-fibers (100 Fibers)	34
7	7 CONCLUSIONS	36
8	REFERENCES	37
9	ELIST OF FIGURES	39
J		



1 EXECUTIVE SUMMARY

This deliverable presents a comprehensive analysis of oxygen (O_2) and carbon dioxide (CO_2) transfer in hollow fiber membranes, focusing on optimizing fiber geometry and flow configurations to enhance mass transfer. The study uses Computational Fluid Dynamics (CFD) simulations to explore the effects of different fiber shapes under transverse and parallel flow configurations, including cylindrical and sinusoidal designs. Key geometrical parameters such as amplitude, rotational orientation, and fiber twisting are investigated to understand their influence on gas exchange performance. The results reveal sinusoidal fibers with complex surface structures can theoretically offer higher mass transfer due to a larger gas transfer area. However, they may also introduce flow disturbances that negatively impact mass transfer rates, especially at high Péclet numbers (Pe) where convective transport is dominant.

For the investigated singular and multi-fiber models, the findings indicate that cylindrical fibers generally exhibit superior specific (per mass transfer area) O_2 uptake and CO_2 removal compared to sinusoidal fibers, highlighting the importance of streamlined geometry in optimizing gas transfer in high Pe flows. Additionally, the study shows that the interplay between fiber shape and flow configuration is crucial for achieving superior mass transfer. This research provides valuable insights into fiber design considerations for artificial lungs and blood oxygenators, emphasizing the need for a tailored approach to maximize the efficiency of gas exchange processes.

The results from multi-fiber models demonstrate that sinusoidal fibers significantly improve overall gas transfer rates compared to cylindrical fibers, with sinusoidal 4 fibers showing the highest gains. In the 100-fiber model, the total gas transfer rate increases by 6.85% for O_2 uptake and 6.16% for CO_2 removal, highlighting the potential of larger fiber arrays to enhance gas exchange. Although sinusoidal fibers exhibit lower specific gas transfer values than cylindrical fibers, their higher total gas transfer rate suggests that, with proper optimization of fiber design and spatial arrangement, they can outperform cylindrical fibers in total gas transfer rate. Furthermore, exploring alternative flow configurations, such as diagonal flow with an angle of attack, could further improve gas exchange by promoting better fluid mixing and reducing stagnation zones. These findings point to sinusoidal fibers as a promising solution for enhancing ECMO system performance when combined with optimized flow dynamics.

2 KEYWORD LIST

BioMembrOS

Biomimetic Membrane

Carbon Dioxide Removal

Computational Fluid Dynamics

Diffusion Coefficients

European Union's Horizon

Extracorporeal Membrane Oxygenation

Fiber Geometry

Gas Exchange Efficiency

Hemolysis Index

Hollow Fiber Membrane

Mass Transfer

Non-Newtonian Blood Model

Organ Support

Oxygen Uptake

Partial Pressure

Pathfinder

European Innovation Council

Sinusoidal Fibers

Cylindrical Fibers

Multi-Fiber Arrangement

Blood-Oxygenator Interface

Specific Carbon Dioxide Removal

Specific Oxygen Uptake



3 LIST OF ACRONYMS

BioMembrOS Biomimetic Membranes for Organ Support

EIC European Innovation Council
CFD Computational Fluid Dynamics

O₂ Oxygen

CO₂ Carbon Dioxide

Re Reynold Number

Pe Péclet Number

PMP Poly (4-Methyl-1-Pentene)

ECMO Extracorporeal Membrane Oxygenation

RBC Red Blood Cell HI Hemolysis Index

Latin Symbols

a Amplitude of Sinusoidal Fibers $[\mu m]$ r Radius of Sinusoidal Fibers $[\mu m]$

n Number of Waves for Sinusoidal Fibers [-]

b Yasuda Parameter [-]
m Power-law Index [-]
v Velocity of Fluid [m/s]

D Average Diameter of Fibers [m] **v** Velocity Vector of Fluid [rad]

 D_i Diffusion Coefficient of Transported Gas Through Membrane $[m^2/s]$

 K_{m} Membrane Permeation [m/(s.mmHg)]

t Time [s]

p Pressure Field [Pa]

 D_{CO_2} Diffusivity of Carbon Dioxide in Blood $[m^2/s]$

 P_{0_2} Oxygen Partial Pressure [mmHg]

 P_{CO_2} Carbon Dioxide Partial Pressure [mmHg]

C Empirical Coefficient for Hemolysis Index Model [-]

 D_{i,O_2} Diffusivity of Oxygen in Membrane $[m^2/s]$

 D_{i,CO_2} Diffusivity of Carbon Dioxide in Membrane $[m^2/s]$

th Thickness of Membrane [m]

Greek Symbols

Angle $[rad]$
Viscosity of the Fluid at Zero Shear Rate $[Pa.s]$
Viscosity of the Fluid at Infinite Shear Rate $[Pa.s]$
Time Constant in the Carreau-Yasuda Model $[s]$
Shear Rate $[s^{-1}]$
Effective Porosity $[-]$
Density of the Fluid $[kg/m^3]$
Empirical Coefficient for Hemolysis Index Model $[-]$
Empirical Coefficient for Hemolysis Index Model [—]
Scalar Shear Stress $[Pa]$



4 INTRODUCTION

This document presents Deliverable D3.1, "Fiber Design Model" for the EIC Pathfinder Open project, BioMembrOS. The primary objective of this deliverable is to modify and optimize the structure of the outer surface and the shape of the inner lumen of the membrane fibers to reduce mass transport resistance. Enhancing these characteristics aims to improve gas exchange efficiency, specifically O_2 uptake and CO_2 removal per volume, which are crucial in applications such as artificial lungs or blood oxygenators.

To reach this objective, detailed CFD simulations are conducted on single and multiple fibers (20 and 100 fiberS) with a sinusoidal outer surface. Single fiber simulation is performed under various flow configurations, including both parallel and transverse flows. These simulations evaluated the transport of O₂ and CO₂ across the membrane. The study also investigates the impact of different parameters, including the amplitude and the number of waves in the sinusoidal structure, on the mass transport performance. Additionally, twisted fibers (with different fiber geometries) are examined to assess their effect on gas exchange efficiency. Specific O₂ uptake and CO₂ removal are calculated and compared across different fiber shapes, including a standard cylindrical fiber and various sinusoidal designs. This comprehensive analysis provides valuable insights into how structural modifications of membrane fibers could improve blood flow conditions and gas exchange performance.

The methodology contained in this study provides a comprehensive analysis of O₂ and CO₂ transfer in hollow fiber membranes, employing various models ranging from simplified to more complex representations of blood and sweep gas dynamics. This approach is applied to different fiber shapes and flow configurations, ensuring a thorough evaluation of mass transfer performance across various conditions.

5 METHODOLOGY

5.1 CFD Domain

CFD simulations are conducted for a single hollow fiber, 20 hollow fibers, and 100 hollow fibers with an average diameter of 400 microns. Multiple fibers, such as 20 or 100, were simulated to capture the interaction effects between fibers, which cannot be observed in a single-fiber simulation. Two fiber shapes are considered in the simulations: cylindrical and sinusoidal. The sinusoidal shape is generated by applying a sinusoidal function around the circular cross-section of the fiber. The radius of the sinusoidal curve is determined using the following equation (r is the radius of the sinusoidal curve, r_{avg} is the average radius, a is the amplitude, a is the number of waves, and a is the angle range from 0 to a to a

$$r(a, n, \theta) = r_{avg} + a \times \sin(n \times \theta)$$
 (1)

Figure 1 shows the CFD domain along with the dimensions and boundaries in both transverse and parallel flow configurations of a single fiber (red area: inlet, green area: outlet, blue area: fiber, and gray area: wall):

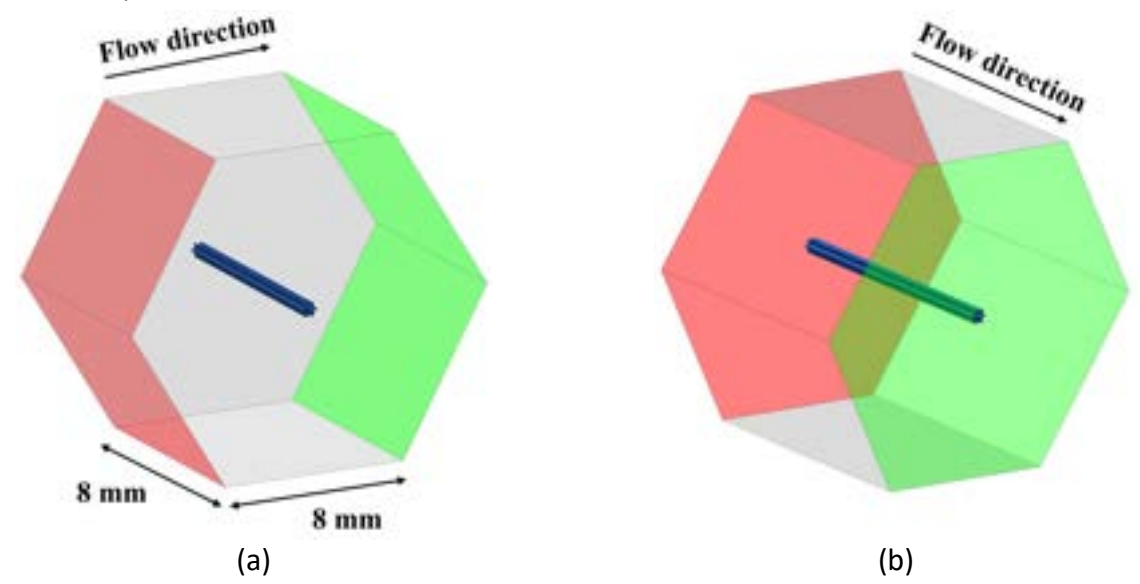


Figure 1. CFD domain with boundaries and dimensions for a single fiber; a) Transverse flow, b) Parallel flow

For 20 and 100 fibers, only the transverse flow configuration is considered. Figure 2 shows the CFD domain with 20 fibers, and Figure 3 shows the CFD domain with 100 fibers along with the dimensions (red area: inlet, green area: outlet, blue area: fiber, and yellow area: symmetry). The fiber's inner lumen shape is considered cylindrical in the CFD models. The inner lumen shape can be sinusoidal as well. Still, in this study, cylindrical shape is only considered to show the effectiveness of the CFD model and its capabilities in the study of gas transfer in different fiber shapes. In the multi-fiber models, the fibers are arranged in a staggered configuration with a center-to-center spacing of 600 microns.



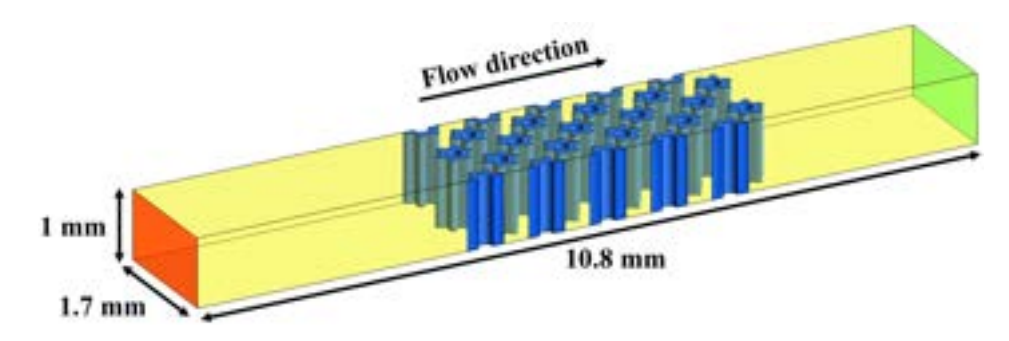


Figure 2. CFD domain with boundaries and dimensions for 20 fibers

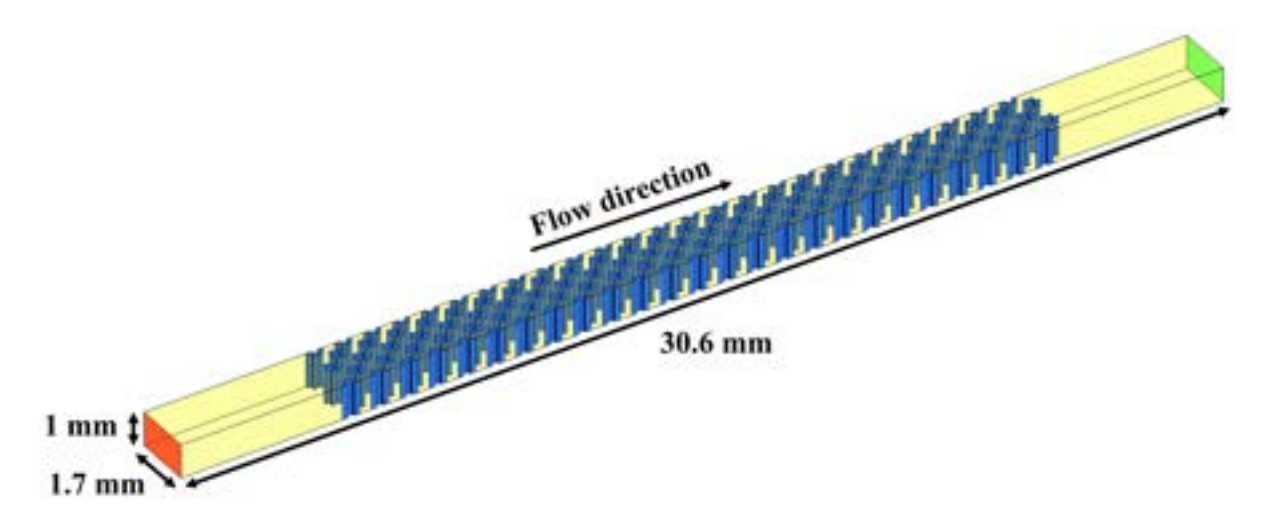


Figure 3. CFD domain with boundaries and dimensions for 100 fibers

5.2 Fluid Physical Properties and Investigated Conditions

Blood is assumed to be non-Newtonian with the Carreau-Yasuda model for viscosity. The Carreau-Yasuda model is well-suited for describing blood flow in the very low Re region (Re < 1) because it accurately captures blood's shear-thinning behavior [1]. In this region, blood shows significant changes in viscosity depending on the shear rate, with its viscosity decreasing as the shear rate increases. The Carreau-Yasuda model effectively represents this behavior across a wide range of shear rates, particularly at low shear rates typical of slow, small-scale flows [2]. Its flexibility and additional parameters allow for precise modeling of blood's complex rheology, making it ideal for low Re applications like microcirculatory flow. The following equation gives the Carreau-Yasuda model:

$$\mu(\dot{\gamma}) = \mu_{\infty} + (\mu_0 - \mu_{\infty})[1 + (\lambda \dot{\gamma})^b]^{(m-1)/b}$$
 (2)

Where:

- $\mu(\dot{\gamma})$ is the apparent viscosity as a function of the shear rate,
- μ_0 is the viscosity at zero shear rate (the low-shear viscosity),
- μ_{∞} is the viscosity at infinite shear rate (the high-shear viscosity),
- λ is the time constant,
- b is the Yasuda parameter that defines the transition sharpness between Newtonian and power-law regions,

- m is the power-law index indicating the degree of shear-thinning behavior,
- $\dot{\gamma}$ is the shear rate.

Figure 4 shows the difference between different non-Newtonian models.

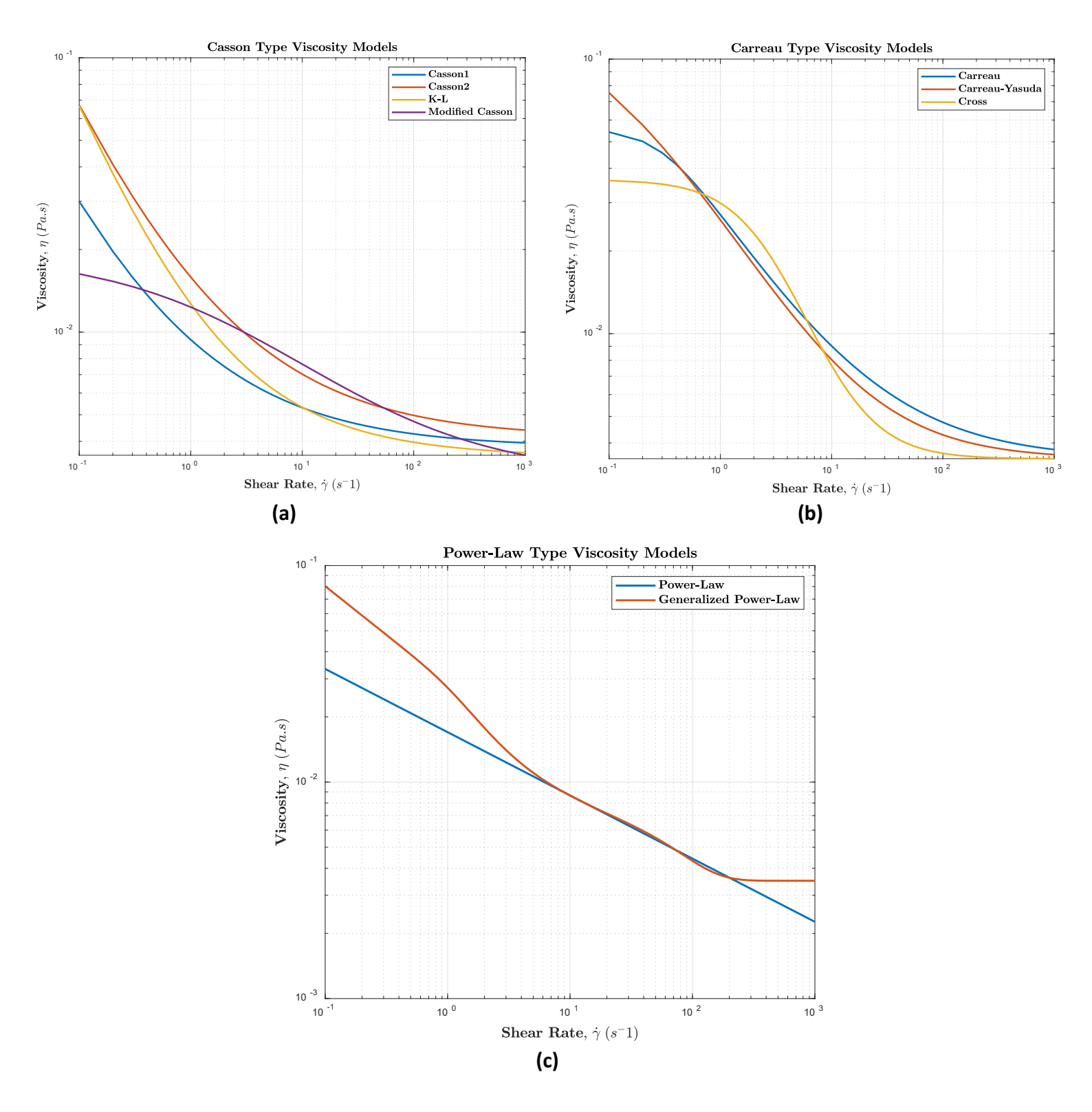


Figure 4. Different non-Newtonian models for blood viscosity. a) Casson type models, b) Carreau type models, c)

Power-law models



The density of the blood was assumed to be 1050 kg/m³. The velocity of the blood was calculated based on the Reynolds number, Re. In Ecker's study of potential fiber shapes for extracorporeal membrane oxygenators, they compared the Sherwood number for sinusoidal and cylindrical fibers at a Re of 0.8 [3]. The Reynolds number for blood flow in the hollow fibers on the blood side of an ECMO circuit typically falls within the low Reynolds number regime due to the fibers' relatively small diameter and the low blood flow velocity. In such systems, the Reynolds number is often less than 1 [4]. So, in this study, the Re is considered to be 0.5, and the blood velocity is calculated as follows:

$$Re = \frac{\rho \ v \ L}{\mu_{\infty}} \rightarrow v = \frac{Re \ \mu_{\infty}}{\rho \ L} = \frac{0.5 \times 0.0035}{1050 \times 400 \times 10^{-6}} = 0.0042 \ m/s$$
 (3)

In the given equation, L represents the characteristic length, which, in this context, refers to the outer diameter of the cylindrical fiber. Since the viscosity varies across the domain due to the Carreau-Yasuda model, the calculation of the Re is based on the viscosity at an infinite shear rate.

Four different scenarios are carried out to examine the impact of various boundary conditions: simulations including only blood flow with either constant partial pressure or applied flux on the outer fiber wall; simulations of both blood flow and membrane with constant partial pressure on the inner fiber wall; and simulations involving airflow inside the fibers along with blood flow on the outside in the presence of the membrane.

In the full model with sweep gas (air), the flow rate ratio of sweep gas to blood flow rate (V/Q) was assumed to be 1 [5]. Furthermore, the diffusion coefficient of O_2 and CO_2 in the blood and air is constant. The diffusion coefficients of O_2 and CO_2 in the membrane are calculated using the Knudsen equation, which accounts for gas transport in porous media [6]. Equation 4 represents the Knudsen equation:

$$D_i = K_m \frac{\tau}{\varepsilon} h \left(\frac{T}{T_0}\right) P_0 \tag{4}$$

Where:

- K_m is the membrane permeation,
- τ is the tortuosity,
- ε is the effective porosity of the membrane,
- *h* is the effective pore diameter,
- T is the blood flow temperature,
- T_0 is the standard temperature,
- P_0 is the standard pressure.

The selected membrane for this study is the 3M Membrana Oxyplus type PMP 90/200. Membrane permeation values for O_2 and CO_2 and other parameters for calculating the diffusion coefficient of gases in the membrane were obtained from the literature [7] to accurately represent gas transport properties through this specific membrane type. Tortuosity, effective porosity, and effective pore diameter are assumed to be 4, 0.4, and 0.03 microns, respectively. Blood temperature is assumed to be 310 K, and standard temperature and pressure are 298 K and 760 mmHg, respectively.

Table 1 summarizes the parameters and coefficients used in the simulations, including the constants for the Carreau-Yasuda model, blood and air density, flow conditions, and diffusion coefficients for O_2 and CO_2 in both blood and air.

Parameters	Value	Unit	Reference
Blood density	1050	kg/m^3	[9]
Air density	1.224	kg/m^3	[10]
Zero-shear viscosity of blood	0.16	Pa.s	[11]
Infinite-shear viscosity of blood	0.0035	Pa.s	[11]
Time constant for blood viscosity	8.2	S	[11]
Yasuda parameter	0.64	_	[11]
Power-law index	0.2128	-	[11]
Blood Velocity	0.0042	m/s	-
Air Viscosity	1.789×10^{-5}	Pa.s	[10]
O ₂ diffusivity in blood	1.8×10^{-9}	m^2/s	[8]
CO ₂ diffusivity in blood	7.39×10^{-10}	m^2/s	[8]
O ₂ diffusivity in air	1.98×10^{-5}	m^2/s	[12]
CO ₂ diffusivity in air	1.6×10^{-5}	m^2/s	[12]
O ₂ diffusivity in membrane	2.53×10^{-9}	m^2/s	[6], [7]
CO ₂ diffusivity in membrane	3.46×10^{-9}	m^2/s	[6], [7]

Table 1. Fluid dynamic parameters used in this study

5.3 Governing Equations and Boundary Conditions

The Navier-Stokes equations express the momentum conservation on a differential control volume. Their numerical solution with appropriate initial and boundary conditions provides the velocity vector and the pressure in each control volume of the discretized computational domain. Since ECMO involves the transport of gases (O₂ and CO₂) through a blood-oxygenator interface, fluid dynamics play a central role in determining how efficiently the gases dissolve and diffuse into or out of the blood. The Navier-Stokes equations for an incompressible fluid (which is a reasonable assumption for blood and air) are given by:

$$\nabla \cdot \mathbf{v} = \mathbf{0} \tag{5}$$

$$\rho \left(\frac{\partial \mathbf{v}}{\partial t} + \mathbf{v} \cdot \nabla \mathbf{v} \right) = -\nabla p + \mu \nabla^2 \mathbf{v} + \mathbf{f}$$
 (6)

Where:

- **v** is the fluid velocity vector,
- ρ is the density of the fluid,
- *p* is the pressure,
- μ is the dynamic viscosity of the fluid,
- **f** is the body force per unit volume, which can include external forces like gravity or magnetic forces, but in ECMO, this term may be negligible.



In ECMO, blood is actively pumped through a membrane oxygenator. The Navier-Stokes equations are essential because they allow us to model how blood flows over the membrane, influencing gas exchange efficiency.

The transport of O_2 and CO_2 in ECMO is governed by fluid flow and mass transfer across the membrane. Fick's law of diffusion can describe the mass transfer of these gases across the membrane. Partial pressure equations are derived based on the idea that gases diffuse from regions of higher partial pressure to regions of lower partial pressure. Typically, gas transport equations are formulated in terms of concentration. However, by applying Henry's Law, the concentration can be expressed as the product of partial pressure and solubility. So, the transport equations can be reformulated in terms of partial pressures, providing a more direct approach for systems where pressure gradients drive gas exchange. The gas transfer equations for O_2 and CO_2 are given by:

$$\mathbf{v}. \nabla P_{\mathbf{O}_2} = D_{\mathbf{O}_2}. \nabla^2 (P_{\mathbf{O}_2}) \tag{7}$$

$$\mathbf{v}.\,\nabla P_{\mathrm{CO}_2} = D_{\mathrm{O}_2}.\,\nabla^2 (P_{\mathrm{CO}_2}) \tag{8}$$

Where:

- D_{O_2} is the diffusivity of oxygen in the fluid.
- P_{O_2} is the partial pressure of oxygen in the fluid.
- D_{CO₂} is the diffusivity of carbon dioxide in the fluid.
- P_{CO_2} is the partial pressure of carbon dioxide in the fluid.

In this deliverable, the initial plan proposed modeling blood as a two-phase non-Newtonian fluid, with platelets represented as spherical solid particles, and incorporating the calculation of platelet stress loading. This approach aimed to account for the combined effects of stress and exposure time concerning shear-induced platelet activation. However, recent research and findings suggest that such a detailed two-phase flow model may not be essential for evaluating hemolysis, which primarily focuses on red blood cell (RBC) damage caused by mechanical forces.

Two-Phase Flow Modeling and Platelet Stress Loading:

A two-phase flow model, which tracks interactions between plasma (the liquid phase) and platelets (the solid phase), is generally used to simulate platelet behavior under mechanical stress. This method effectively predicts platelet activation and aggregation due to shear forces, as seen in high-stress environments like extracorporeal circuits. Platelet activation occurs when they are subjected to high shear stress over a prolonged time, a phenomenon central to shear-induced platelet activation.

While the two-phase flow model offers a highly detailed approach by incorporating platelets, it may be more than necessary when the primary focus is hemolysis, which involves the rupture of red blood cells (RBCs) rather than platelet activation. In ECMO systems, hemolysis is predominantly driven by mechanical stress on RBCs, mainly due to shear forces and exposure time, rather than platelet interactions. Therefore, including platelets as a separate phase in the simulation is not critical for accurately understanding and predicting RBC destruction.

- Hemolysis Index for Evaluating Hemolysis:

An approach for evaluating hemolysis is using a hemolysis index (HI), simplifying the relationship between shear stress, exposure time, and red blood cell damage. Hemolysis is often evaluated using empirical models that relate the mechanical stress and time of exposure to the degree of RBC lysis. This approach has been validated in numerous studies and provides a more direct and computationally efficient method for assessing hemolysis. The hemolysis index (HI) is typically expressed as [13]:

$$\frac{\partial HI'}{\partial t} + (\mathbf{v}.\nabla) HI' = (C \sigma^{\beta})^{1/\alpha}$$
(9)

Where:

- HI can be calculated from the HI' as follows: HI = $HI'^{1/\alpha}$,
- C, α , and β are the empirical coefficients,
- σ is the scalar shear stress (see Equation 10).

$$\sigma = \left[\frac{1}{6} \sum_{i \neq j} (\tau_{ii} - \tau_{jj})^2 + \sum_{i=j} \tau_{ij}^2 \right]^{1/2}$$
 (10)

Where τ_{ij} is the shear stress tensor.

5.3.1 Boundary Condition Study

To accurately evaluate the boundary conditions for O_2 and CO_2 transfer, a set of simulations is performed for four different scenarios, applying distinct boundary conditions to a single cylindrical fiber and sinusoidal fiber with 3 and 6 waves with an amplitude of 50 microns. These four cases were designed to explore various interactions between the blood, membrane, and gas phases, providing a comprehensive understanding of the mass transfer dynamics across different fiber shapes. The O_2 partial pressure is shown at the x-y and x-z midplanes. Figure 5 shows the mentioned midplanes:



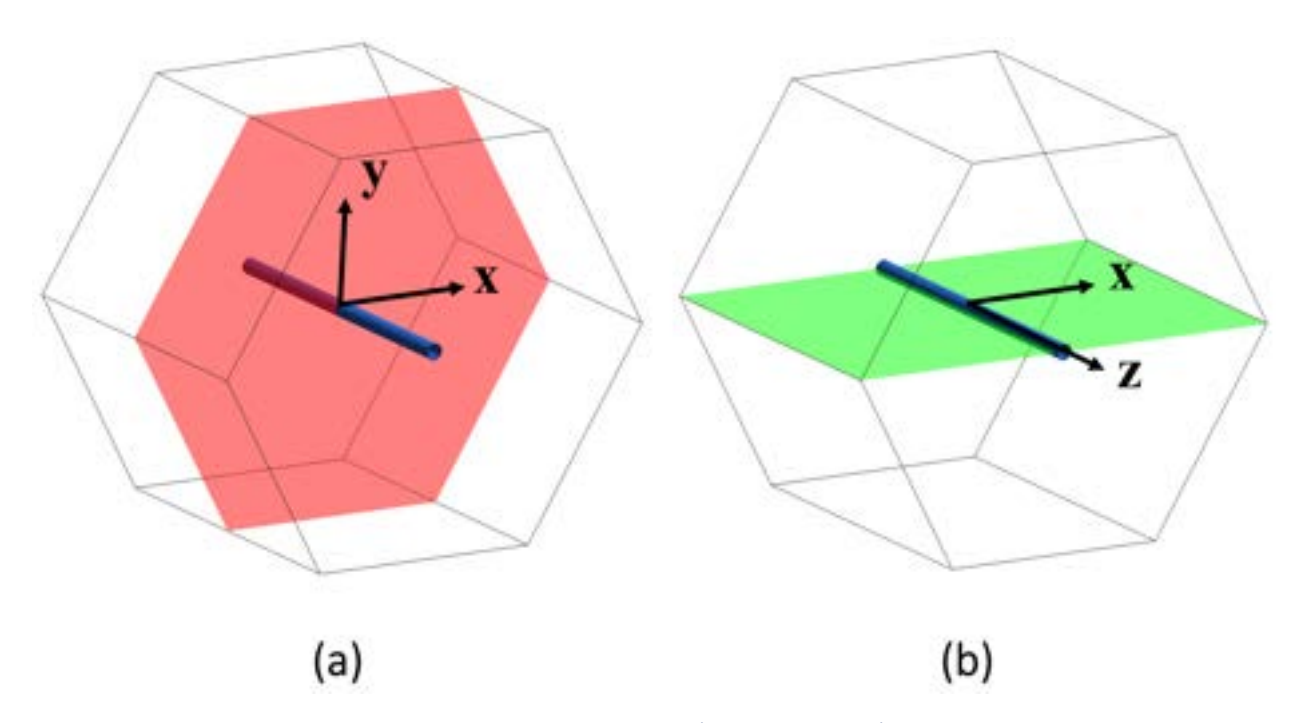


Figure 5. Planes to show the results, a) x-y midplane, b) x-z midplane

The scenarios are described as follows:

1. Constant Partial Pressure at the Fiber Outer Wall (Blood Only): In this scenario, a constant partial pressure is applied on the fiber's outer wall. This setup represents a simplified condition, allowing for the evaluation of the mass transfer based solely on the blood phase. Figure 6 shows the result of this scenario for cylindrical fiber on the mentioned midplanes:

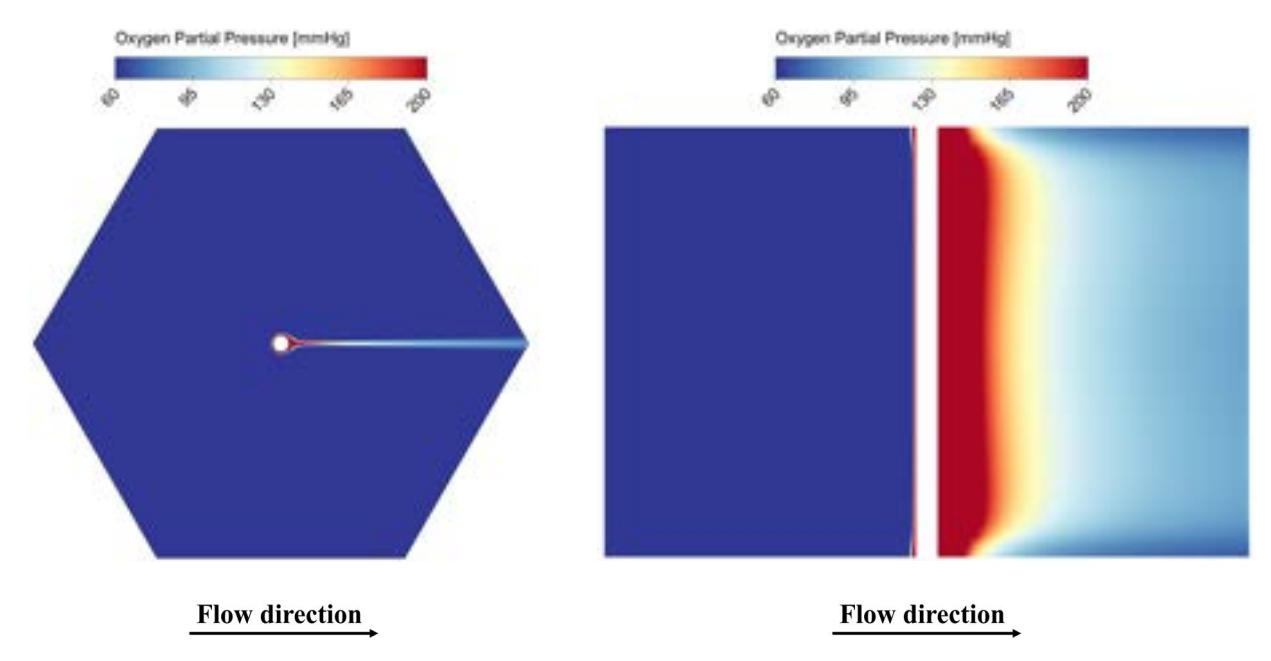


Figure 6. O₂ partial pressure contour at x-y and x-z midplanes for scenario 1

2. Flux Applied to the Fiber Outer Wall (Blood Only): Here, a flux boundary condition was applied at the fiber's outer wall, with the flux being a function of the partial pressure difference and the thickness of the membrane. This approach provided a more dynamic representation of the gas transfer process by considering the influence of the membrane's resistance to mass transfer, even though only the blood phase was simulated. The flux for O₂ and CO₂ is calculated as follows:

$$J_{O_2} = D_{i,O_2} \nabla P_{O_2} = D_{i,O_2} / th \times (700 - P_{O_2})$$
(11)

$$J_{CO_2} = D_{i,CO_2} \nabla P_{CO_2} = D_{i,CO_2} / th \times (700 - P_{CO_2})$$
 (12)

Where J is the flux, D_i is the diffusivity of the gas in the membrane (see Table 1), and th is the thickness of the membrane. For cylindrical fibers, the thickness is 100 microns (based on 3M Membrana Oxyplus), but for sinusoidal fibers, the thickness changes based on position. The limitation of this scenario is that it forces the flux, so there will be flux also in the area where the velocity is minimal (stagnation). Figure 7 shows the result of this scenario:

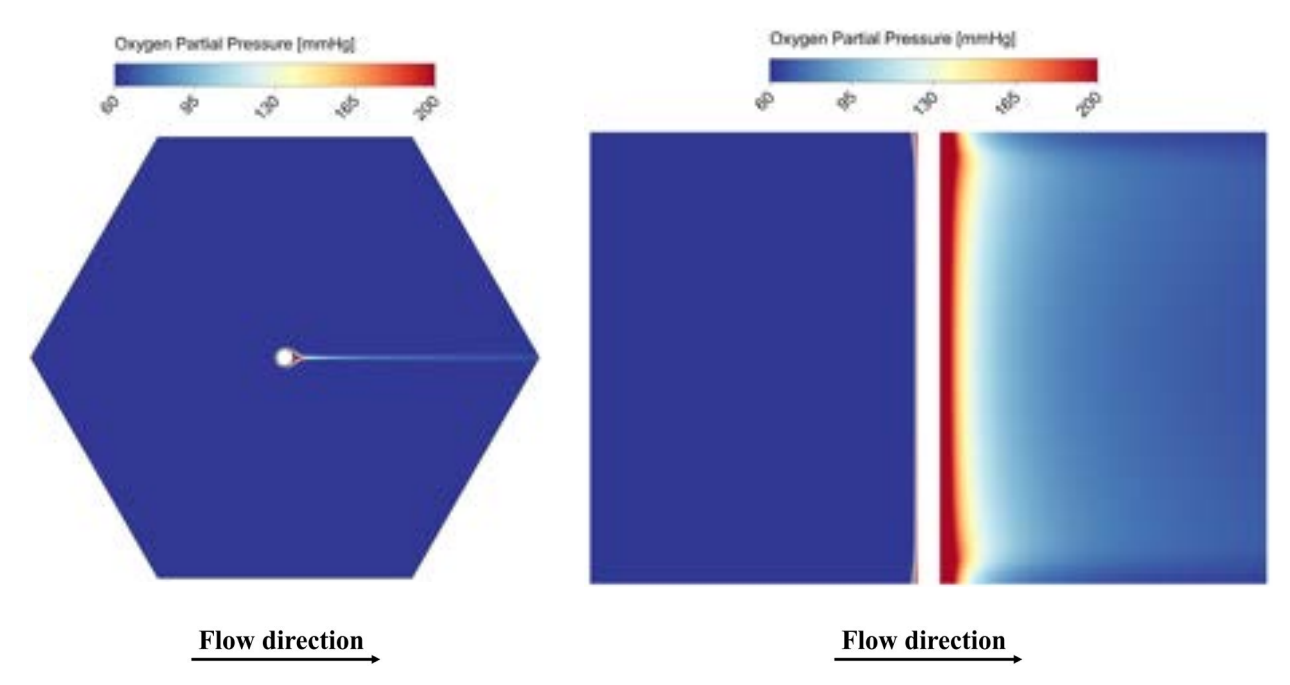


Figure 7. O₂ partial pressure contour at x-y and x-z midplanes for scenario 2

3. Constant Partial Pressure at the Fiber Inner Wall (Blood and Membrane): In this case, the blood and the membrane were simulated, with a constant partial pressure set at the fiber's inner wall. The fluid velocity is assumed to be 0 in the membrane, and the transport equations given in Equations 7 and 8 with the diffusion coefficient of O₂ and CO₂ in the membrane are solved. This setup accounts for the interaction between the blood and the membrane, providing insight into how the membrane's properties affect gas exchange under constant partial pressure conditions within the fiber. Figure 8 shows the result of this scenario:



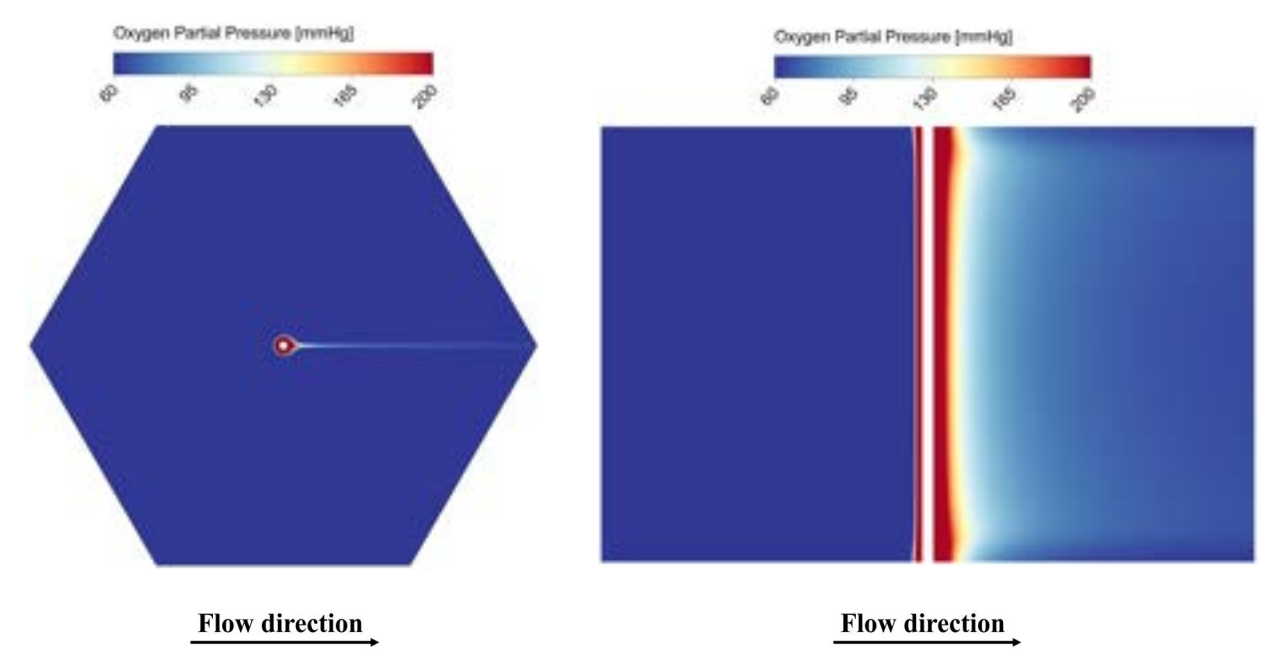


Figure 8. O₂ partial pressure contour at x-y and x-z midplanes for scenario 3

4. Constant Partial Pressure at the Inlet of Sweep Gas (Blood, Membrane, and Air): This more complex model involved the simulation of blood, membrane, and air as a sweep gas. A constant partial pressure was applied at the inlet of the sweep gas, allowing the partial pressure drop at the sweep gas outlet to be observed. This configuration offers a realistic representation of an oxygenator's operation, where the sweep gas is crucial in facilitating gas exchange across the membrane. Figure 9 shows the result of this scenario:

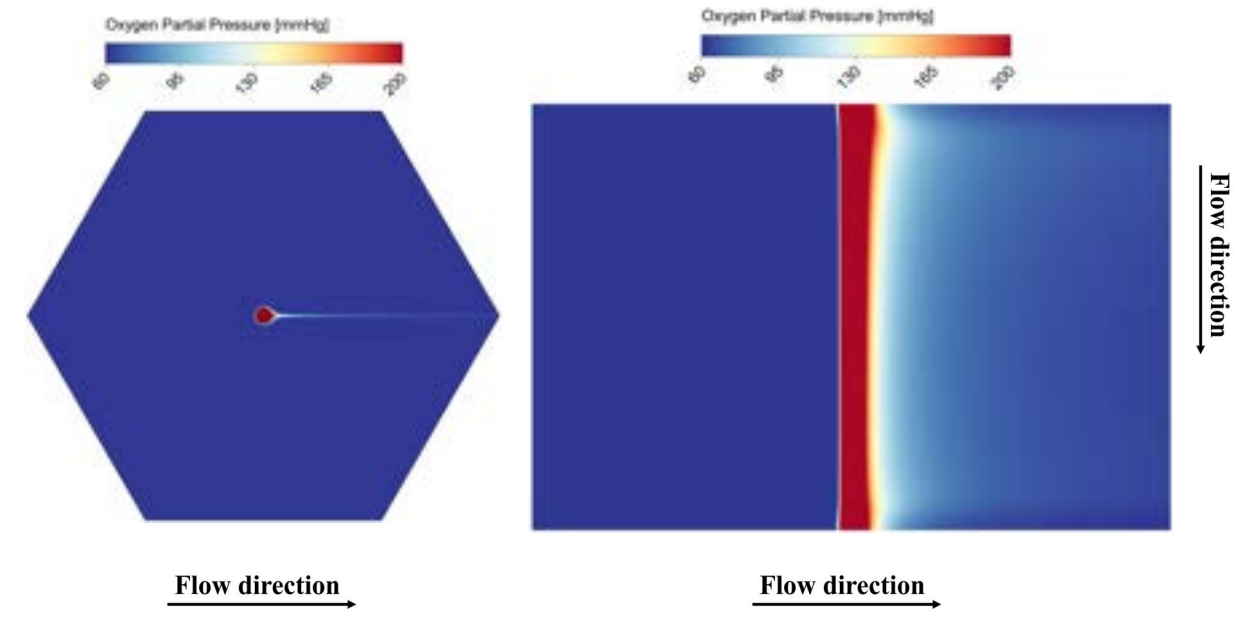


Figure 9. O₂ partial pressure contour at x-y and x-z midplanes for scenario 4

By changing the range of the contour at x-z midplane, the partial pressure drop and gas transfer in the sweep gas side will be more visible, as shown in Figure 10:

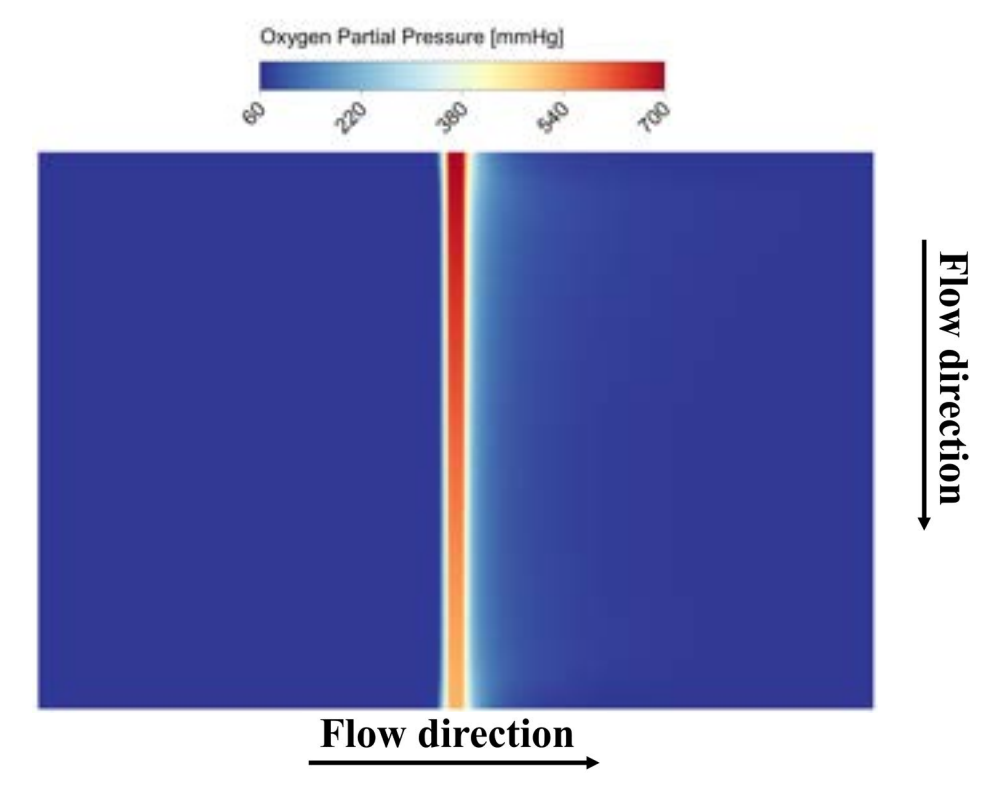


Figure 10. O₂ partial pressure contour at x-z midplane for scenario 4

Tables 2-4 show the result obtained for each scenario with cylindrical, sinusoidal 3, and sinusoidal 6 fibers:

Table 2. Mass transfer results for cylindrical fiber in different scenarios

Scenarios	O ₂ Uptake [ml O ₂ / min]	CO ₂ Removal [ml O ₂ / min]	Specific O_2 Uptake $[ml\ O_2\ /\ min\ /\ m^2]$	Specific CO ₂ Removal $[ml\ O_2\ /\ min\ /\ m^2]$
Scenario 1	5.78E-04	4.60E-04	57.45	45.80
Scenario 2	2.22E-04	2.80E-04	22.06	27.87
Scenario 3	1.79E-04	2.41E-04	17.84	24.00
Scenario 4	1.52E-04	2.00E-04	15.17	19.87

Table 3. Mass transfer results for sinusoidal fiber with 3 waves in different scenarios

Scenarios	O_2 Uptake $[ml\ O_2\ /\ min]$	CO ₂ Removal [ml O ₂ / min]	Specific O_2 Uptake $[ml\ O_2\ /\ min\ /\ m^2]$	Specific CO ₂ Removal $[ml\ O_2\ /\ min\ /\ m^2]$
Scenario 1	5.76E-04	4.56E-04	50.74	40.17
Scenario 2	2.27E-04	2.72E-04	19.94	23.93
Scenario 3	1.74E-04	2.25E-04	15.33	19.78
Scenario 4	1.49E-04	1.87E-04	13.09	16.48



Table 4. Mass transfer results for sinusoidal fiber with 6 waves in different scenarios

Scenarios	O ₂ Uptake [ml O ₂ / min]	CO ₂ Removal [ml O ₂ / min]	Specific O ₂ Uptake [ml O ₂ / min / m ²]	Specific CO ₂ Removal $[ml\ O_2\ /\ min\ /\ m^2]$
Scenario 1	5.54E-04	4.34E-04	38.46	30.13
Scenario 2	2.31E-04	2.61E-04	16.03	18.10
Scenario 3	1.59E-04	2.02E-04	11.03	14.06
Scenario 4	1.38E-04	1.72E-04	9.59	11.94

The results indicated that the simplest model (Scenario 1) exhibited a significant difference in calculating mass transfer compared to the full model (Scenario 4). When using Scenario 4 as the reference full model, which accounts for all material interactions, Scenario 3 (constant partial pressure at the fiber inner wall) demonstrated a close agreement with the results of Scenario 4, suggesting it as a more accurate yet simpler alternative for simulating mass transfer.

5.4 Mesh Dependence Study

A mesh dependence study in CFD is crucial for ensuring that the simulation results are independent of the mesh size and accurately capture the modeled physical phenomena. This study involves refining the mesh and observing changes in O₂ partial pressure at a line after the fiber to determine the point at which further mesh refinement has a negligible impact on the results. This is especially important in cases like this study, where multiple simulations are required to assess the effect of various parameters related to the fiber geometry, such as amplitude, number of waves, etc.

Five different meshes with the number of elements of 350k, 750k, 1500k, 2500k, and 3500k have been evaluated for three different cases:

- 1- Cylindrical fiber
- 2- Sinusoidal 3 with amplitude of 50 microns (number of waves of 3)
- 3- Sinusoidal 6 with amplitude of 50 microns (number of waves of 6)

 O_2 partial pressure at the inlet is set to 56 mmHg, equivalent to the saturation of 65%, and on the fiber is set to 700 mmHg. This boundary condition is the simplest, and it doesn't consider the thickness of the fiber. Figure 11 shows the line where O_2 partial pressure is calculated:

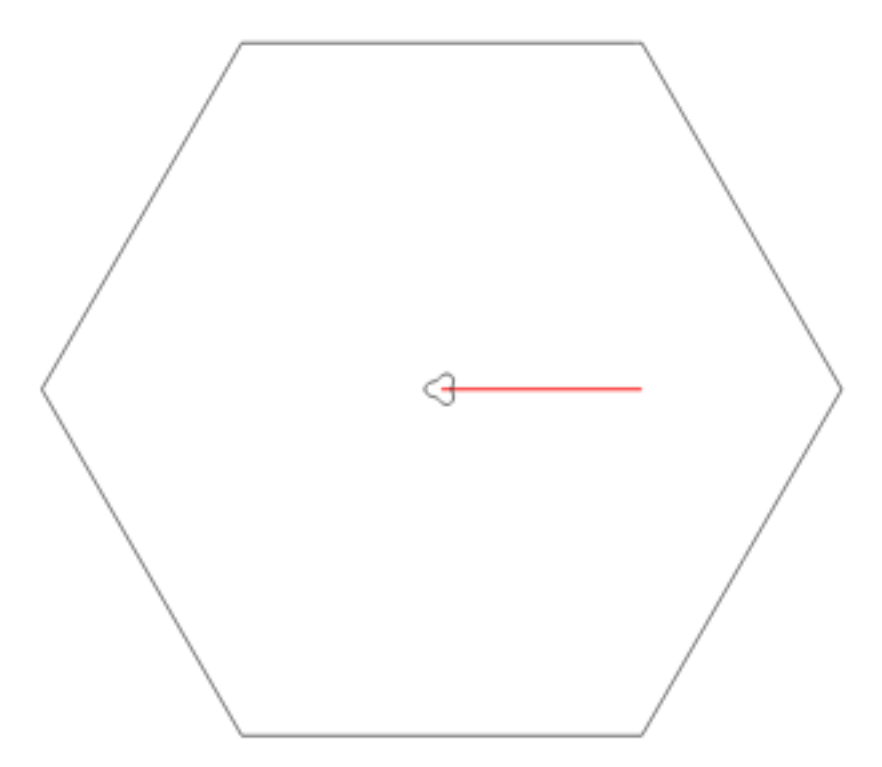


Figure 11. The line for calculating O₂ partial pressure

Each mesh's root mean square error (RMSE) with the finest mesh (3500k) was calculated. Figure 12 shows the O₂ partial pressure at the mentioned line for each case:



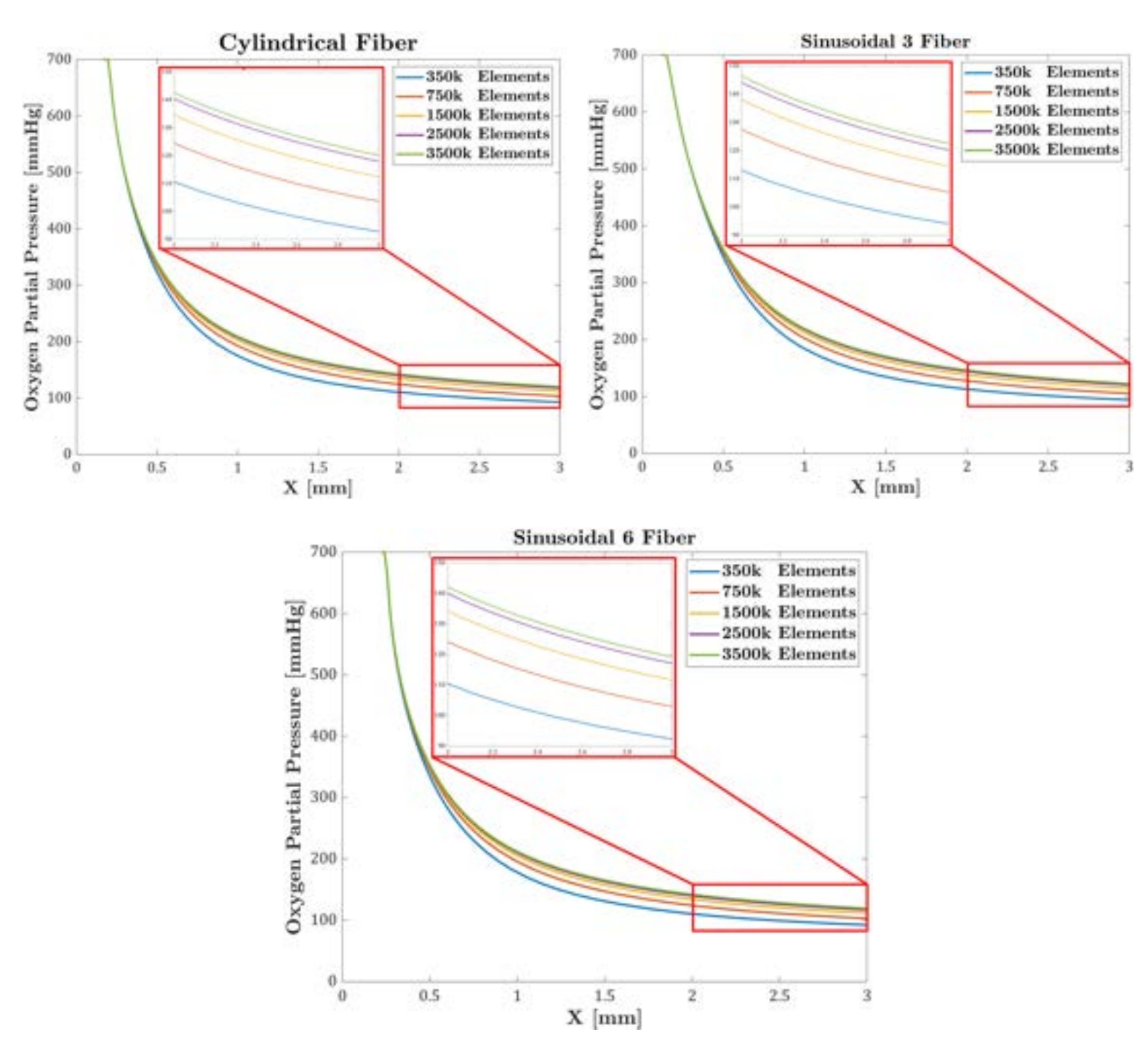


Figure 12. O₂ partial pressure at the mentioned line for different cases and different meshes

The RMSE percentage for each case and different meshes are reported in Table 5:

Table 5. Root mean square error percentage of each mesh for different fibers

Cases	RMSE for 350k [%]	RMSE for 750k [%]	RMSE for 1500k [%]	RMSE for 2500k [%]
Cylindrical Fiber	12.12	6.51	2.81	0.77
Sinusoidal 3 Fiber	11.60	6.24	2.70	0.72
Sinusoidal 6 Fiber	12.59	6.75	2.91	0.78

As shown in Table 5, the difference between 2500k and 3500k element meshes is below 1%, and between 1500k and 3500k element meshes is below 3%. Since the difference in the latter is below 5%, the 1500k element meshes were selected for further simulations. Figure 13 shows the generated mesh with 1500k elements for sinusoidal 6 fibers with an amplitude of 50 microns:

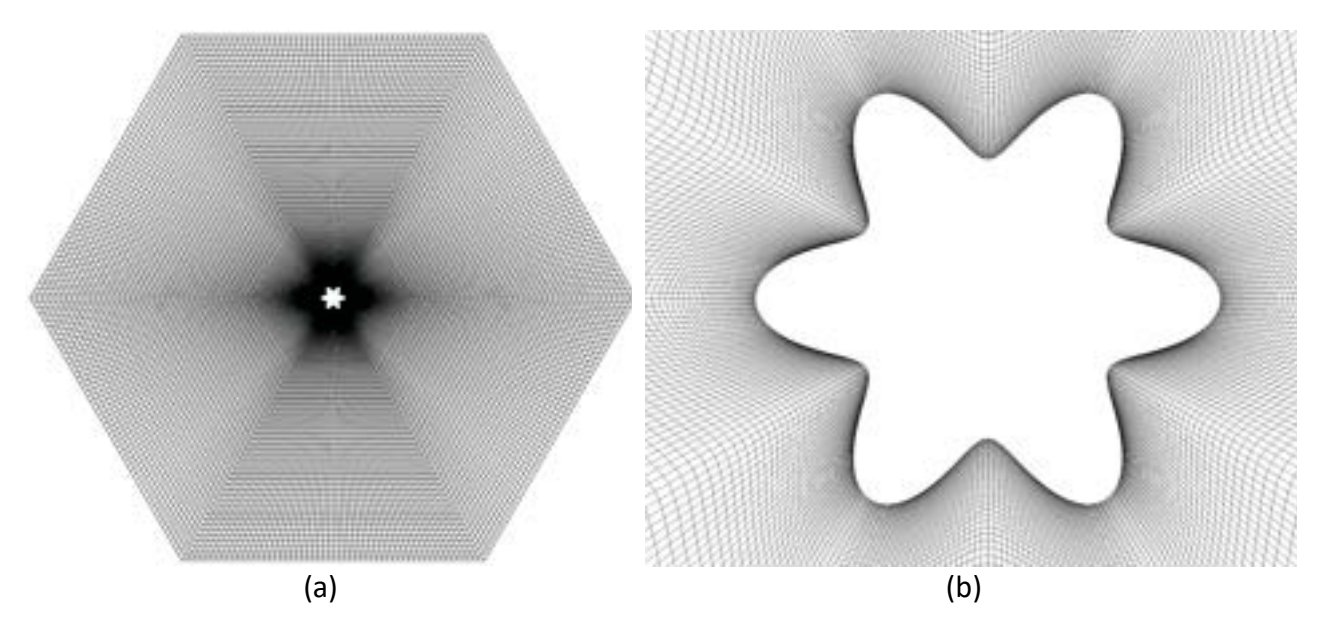


Figure 13. 1500k elements mesh for sinusoidal 6 fiber with amplitude of 50 microns, a) full view, b) zoomed in

The same element size has been used for the geometries with 20 and 100 fibers. A structured mesh with a minimum orthogonal quality of 0.4 is generated in all cases. Figure 14 shows the generated mesh for fibers in the staggered position:

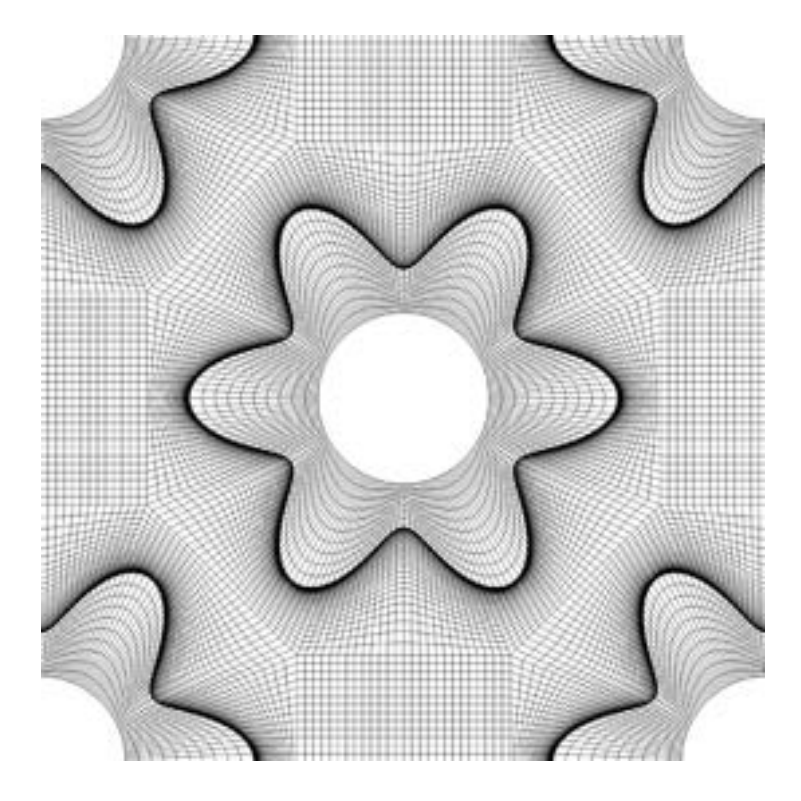


Figure 14. Generated mesh for fibers in a staggered position



6 RESULTS AND DISCUSSION

The simulations are conducted for single and multiple fibers (20 and 100 fibers). Two distinct flow configurations are investigated for single fiber: transverse and parallel flow. Each configuration was analyzed to understand how the different geometric modifications of the fibers affect mass transfer.

Before analyzing the results, it is important to examine the Péclet (Pe) number to determine whether the flow behavior is dominated by diffusion or convection. Pe is a dimensionless number that characterizes the relative importance of convective transport to diffusive transport in a fluid flow. It provides insight into the dominant transport mechanism within the system, whether it is primarily controlled by advection (movement due to the flow) or diffusion (movement due to concentration gradients). The Péclet number is defined as:

$$Pe = \frac{v L}{D_i} \tag{13}$$

Where:

- v is the characteristic velocity of the flow (m/s),
- L is the characteristic length scale (m),
- D_i is the diffusion coefficient of the substance being transported (m²/s).

For flow with a high Pe number, convective transport dominates over diffusive transport. It means that the movement of particles is primarily due to the flow of the fluid rather than diffusion. In such cases, the substance is quickly transported through the system. The Pe number in this study can be calculated as follows (the outer diameter of the cylindrical fiber is considered for the characteristic length):

$$Pe_{O_2} = \frac{0.0042 \times 400 \times 10^{-6}}{1.8 \times 10^{-9}} = 933 \gg 1 \tag{14}$$

With a very high Péclet number (Pe = 933), convective transport is overwhelmingly dominant over diffusive transport. In this regime, the flow primarily drives the mass transfer, and the effectiveness of gas exchange is mainly dependent on the convective movement of the fluid rather than on diffusion. In such scenarios, a more streamlined geometry, like that of a cylindrical fiber, may facilitate a more efficient and uniform flow around the fiber, resulting in better overall mass transfer.

6.1 Single Fiber

6.1.1 Transverse Flow

In this configuration, the fluid flows perpendicular to the length of the fiber. The effects of both the sinusoidal surface structure amplitude and the fiber's rotational orientation were evaluated. The amplitude changes the surface undulation degree, influencing the fiber's flow dynamics. Additionally, the fiber's rotation alters how the fluid interacts with these surface undulations, potentially affecting the convective transport and, consequently, the mass transfer rates of O_2 and CO_2 .

6.1.1.1 Effect of Amplitude

Simulations are performed for different sinusoidal fibers with the number of waves from 3 to 6, varying the amplitude from 10 to 50 microns. Figure 15 shows the O_2 uptake and CO_2 removal for different sinusoidal fibers versus amplitude:

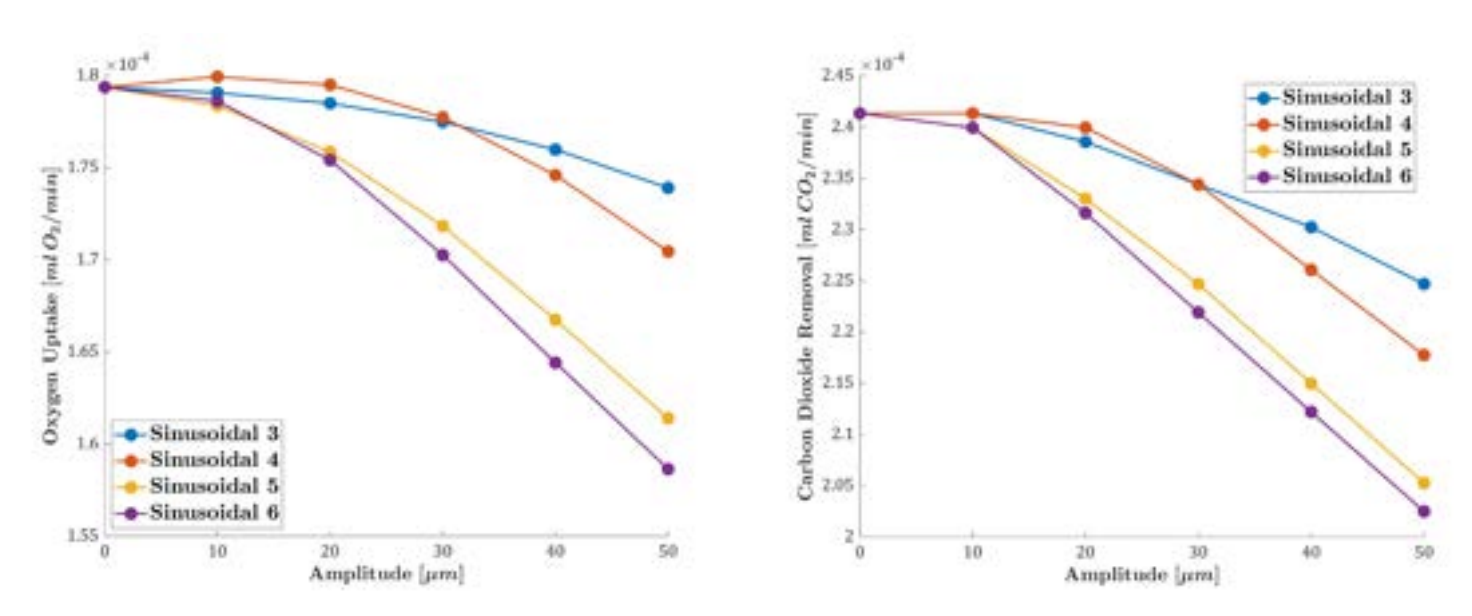


Figure 15. O₂ uptake and CO₂ removal versus amplitude in the transverse flow configuration

Figure 15 indicates that increasing the sinusoidal fibers' amplitude decreases O₂ uptake and CO₂ removal. Increasing the sinusoidal fibers' amplitude introduces a more complex surface topology that increases the surface area. However, higher amplitude results in higher area of stagnation and recirculation. In this study, with a very high Pe, flow disruption results from high amplitudes, resulting in adverse effects on gas transfer. In other words, high amplitude could lead to a thicker boundary layer, limiting the gas transfer efficiency.

Although O_2 uptake and CO_2 removal are two critical factors, the specific O_2 uptake and specific CO_2 removal are crucial factors that present the gas transfer efficiency in the fiber. Specific O_2 uptake and specific CO_2 removal are calculated by dividing the transferred gas by the fiber area. Figure 16



shows the specific O_2 uptake and specific CO_2 removal versus amplitude in transverse flow configuration:

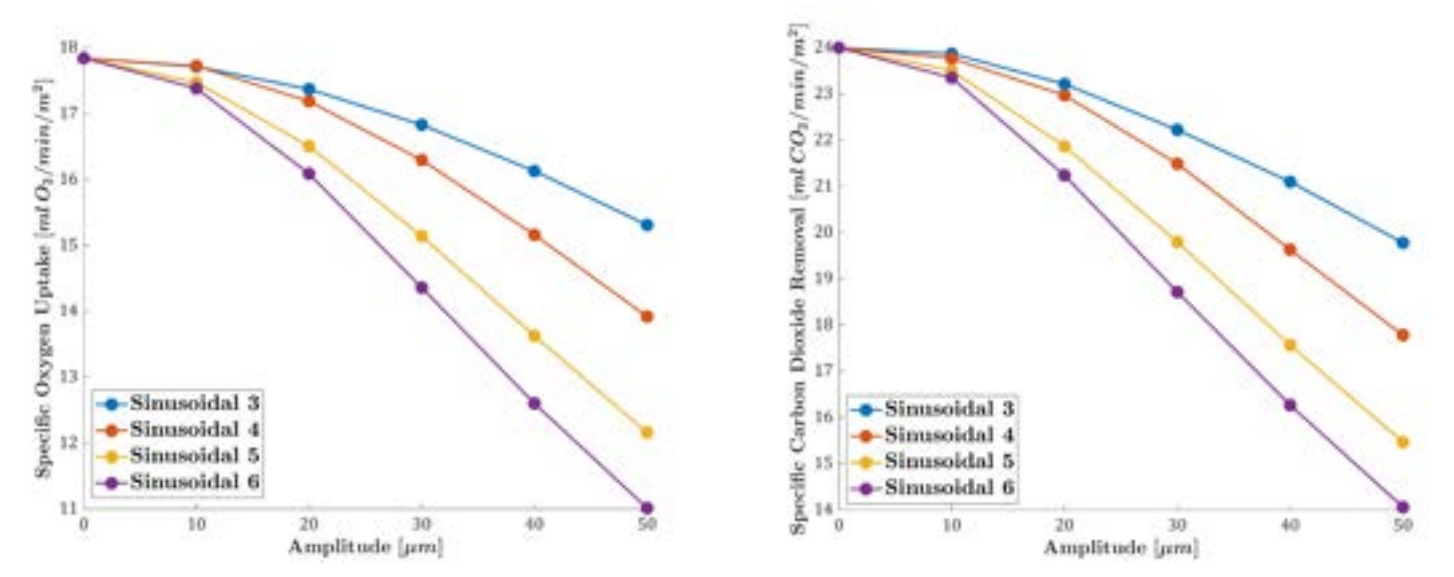


Figure 16. Specific O2 uptake and Specific CO2 removal versus amplitude in the transverse flow configuration

Figure 16 illustrates that the specific gas transfer decreases as the amplitude increases. At lower amplitudes, the differences in gas transfer performance between the sinusoidal fibers are negligible, indicating that the impact of fiber shape becomes less pronounced when the surface undulations are minimal. Also, it can be calculated that the difference between sinusoidal 3 and sinusoidal 6 at the amplitude of 50 microns is around 29%.

Figure 17 shows the specific O₂ uptake and specific CO₂ removal of different sinusoidal with an amplitude of 50 microns in comparison with cylindrical fiber:

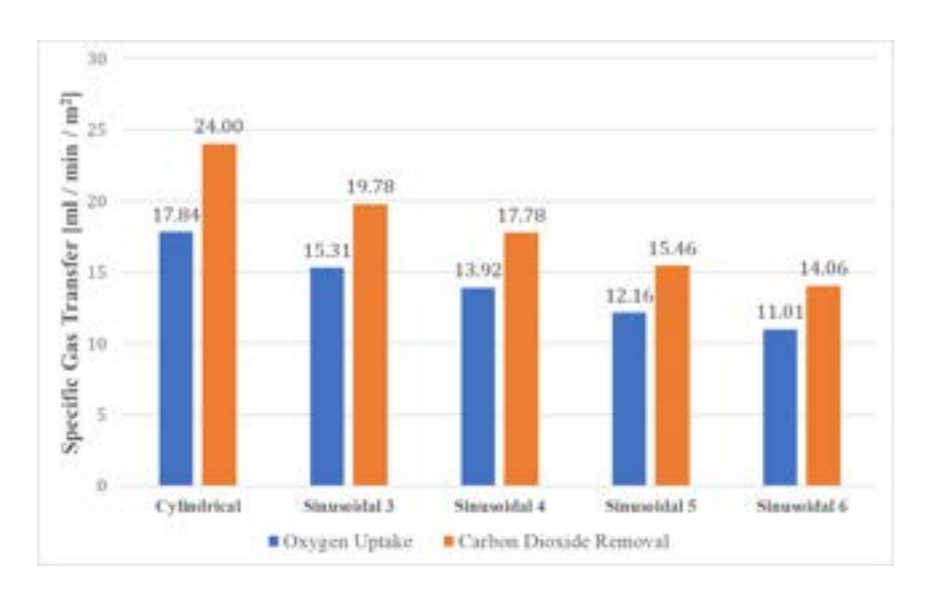


Figure 17. Specific gas transfer for different sinusoidal fibers with an amplitude of 50 microns in comparison with cylindrical fiber

Figure 17 indicates that the cylindrical fibers have the best specific gas transfer compared to sinusoidal fibers with an amplitude of 50 microns. Also, it is shown that the specific CO₂ removal is

higher than the O_2 uptake. The higher specific CO_2 removal compared to specific O_2 uptake is primarily due to the higher solubility and diffusivity of CO_2 .

A closer examination of the data reveals that the O_2 uptake for the sinusoidal fiber with 4 waves and an amplitude of 10 microns (0.00017994 $ml\ O_2\ /min$) is slightly higher than that of the cylindrical fiber (0.00017937 $ml\ O_2\ /min$). However, when considering the specific O_2 uptake, the sinusoidal fiber (17.72 $ml\ O_2\ /min\ /m^2$) exhibits a lower value compared to the cylindrical fiber (17.84 $ml\ O_2\ /min\ /m^2$). This indicates that while the total O_2 uptake may increase slightly for the sinusoidal fiber, the gas exchange efficiency is reduced relative to the surface area.

6.1.1.2 Effect of Rotation

The rotation of the fiber alters the flow behavior around the fiber, similar to introducing an angle of attack in the fluid flow. By changing the orientation of the fiber relative to the incoming flow, the surface exposure and the interaction dynamics between the fluid and the fiber surface are modified. This can either enhance or diminish the overall mass transfer efficiency depending on the angle. For example, certain angles may increase the disruption of the boundary layer, promoting more effective mixing and potentially improving O_2 uptake and CO_2 removal. Conversely, other angles might lead to more extensive wake formation or regions of flow separation, which could reduce gas transfer efficiency by increasing areas of low fluid velocity or stagnation.

Figure 18 shows the effect of rotation on the gas transfer. The angles of rotations are normalized, so 0 represents 0 degrees, and 1 represents (360/n) degrees, where n is the number of waves. For example, a normalized angle of 1 in sinusoidal 3 represents the rotation angle of 120 degrees. An amplitude of 50 microns was used for the sinusoidal fibers.

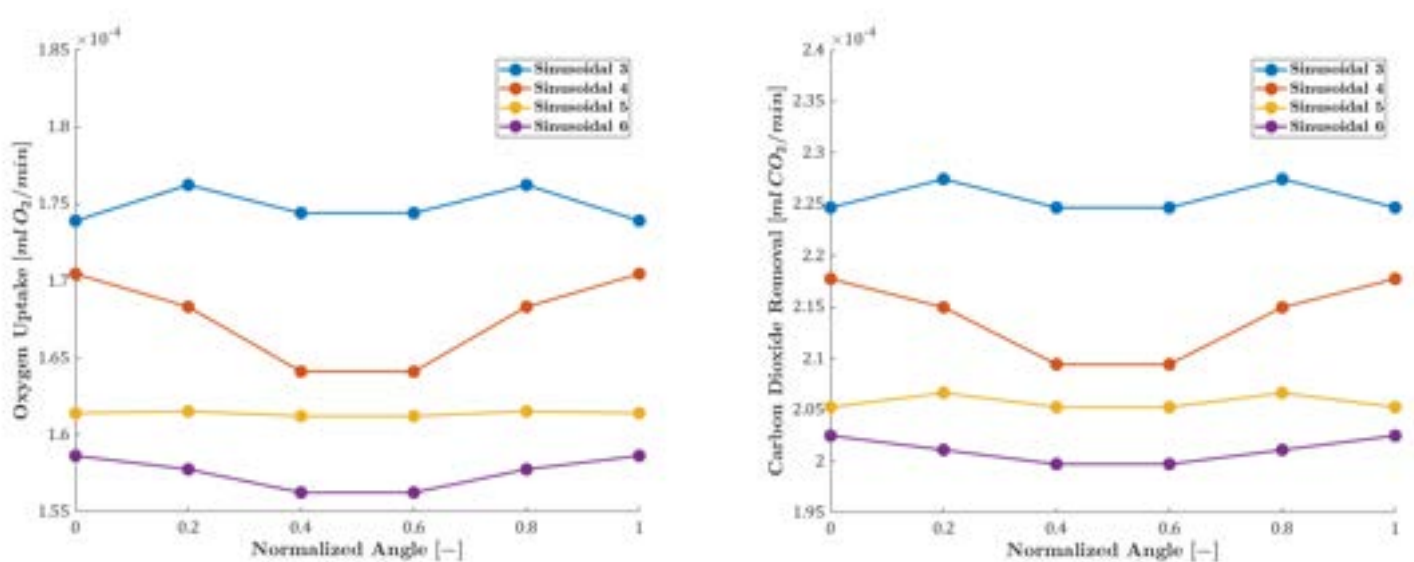


Figure 18. Effect of rotation on O2 uptake and CO2 removal

As it was explained, fiber rotation, in some cases, could increase the gas transfer. This behavior is seen in sinusoidal 3 and sinusoidal 5 fibers. Although sinusoidal 5 doesn't show too much difference.



Besides, sinusoidal 4 and sinusoidal 6 showed an inverse result, so the highest gas transfer in these fibers happens when the flow has no angle of attack. In sinusoidal 3, by rotating the fiber by 24 degrees (normalized angle of 0.2), the O_2 uptake is increased by only 1.33%, which can be negligible. So, it can be concluded that the rotation of the fiber affects the gas transfer, but it's insignificant.

Figure 19 shows the effect of rotation on the specific O_2 uptake and specific CO_2 removal. These results show that rotating the fiber makes the specific gas transfer change negligible.

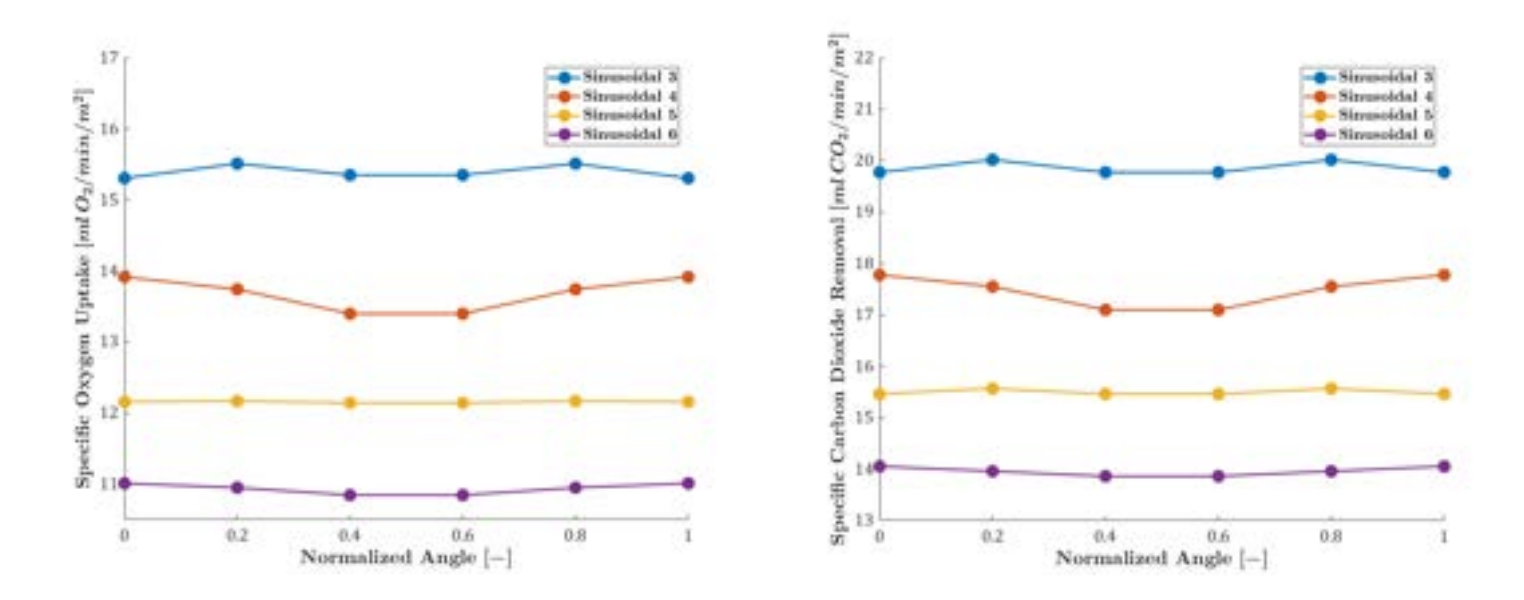


Figure 19. Effect of rotation on specific O₂ uptake and specific CO₂ removal

6.1.2 Parallel Flow

In the parallel flow configuration, the fluid flows along the length of the fiber. The effects of both the sinusoidal surface structure amplitude and the fibers' twisting were evaluated. The amplitude modifies the degree of surface undulation, thereby influencing the flow dynamics along the fiber. Additionally, twisting the fibers introduces a helical geometry, which can alter the interaction between the fluid and the fiber surface. This twisting can enhance mixing and disrupt boundary layers, potentially improving the convective transport and, consequently, the mass transfer rates of O₂ and CO₂.

6.1.2.1 Effect of Amplitude

Similar to transverse flow, simulations have been done for different sinusoidal fibers with the number of waves from 3 to 6, varying the amplitude from 10 to 50 microns. Figure 20 shows the O₂ uptake and CO₂ removal for different sinusoidal fibers versus amplitude:

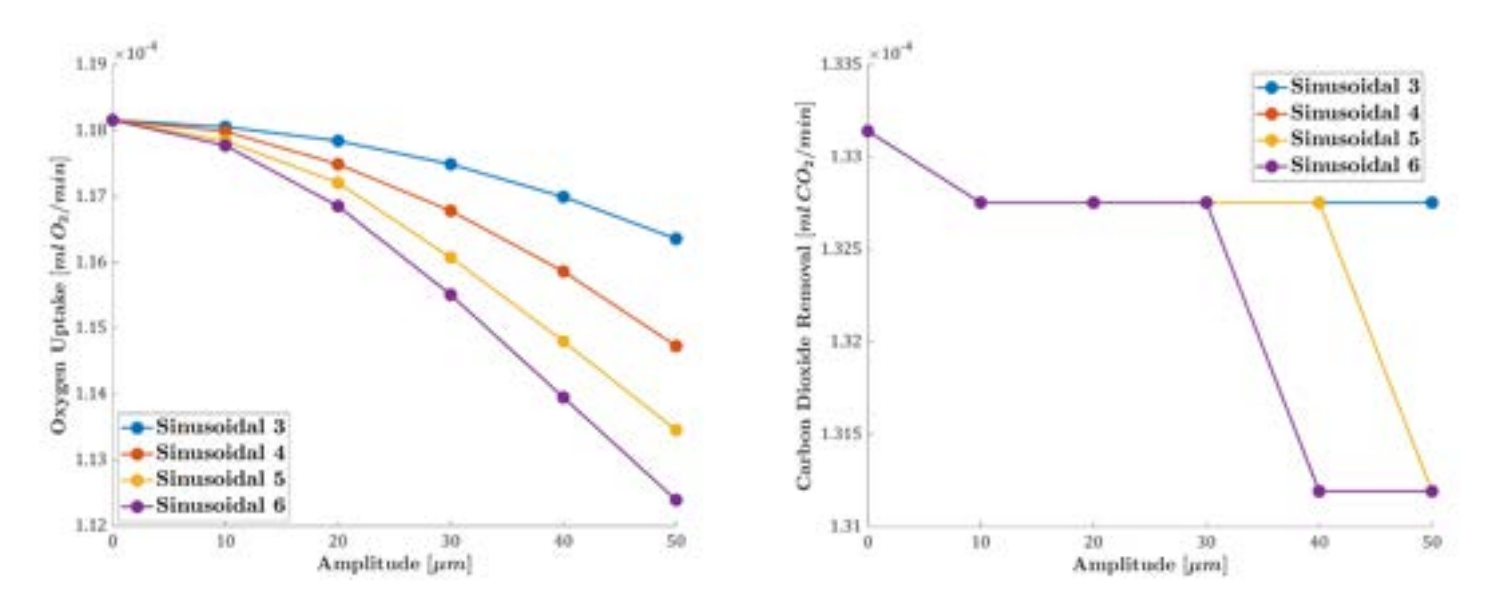


Figure 20. Effect of amplitude on O₂ uptake and CO₂ removal in parallel flow

Figure 20 shows a similar behavior to transverse flow. Increasing the amplitude results in decreasing the O_2 uptake. However, CO_2 removal shows a slight decrease when the amplitude increases, which is negligible. Also, by comparing Figure 20 with Figure 15, it can be concluded that the O_2 uptake and CO_2 removal are much higher in transverse flow than in parallel flow.

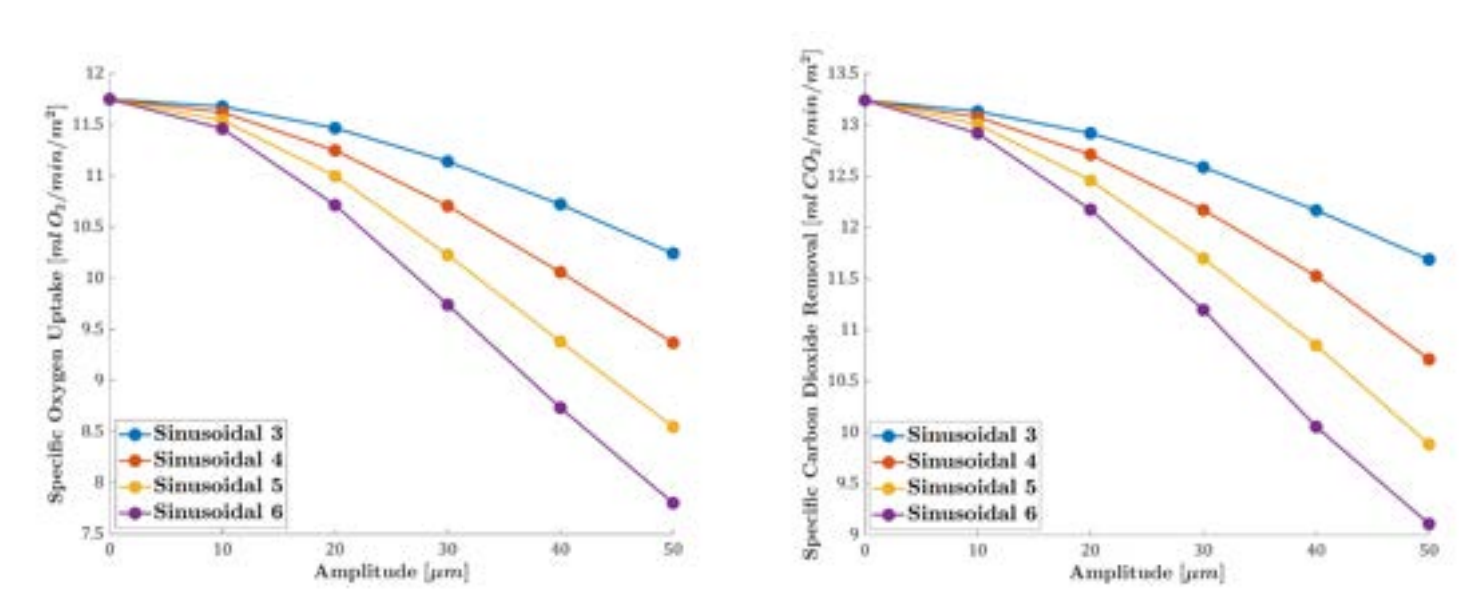


Figure 21. Effect of amplitude on specific O2 uptake and specific CO2 removal in parallel flow



Figure 21 shows the effect of amplitude on specific O_2 uptake and specific CO_2 removal, in which, in both of them, the specific gas transfer decreases by increasing the amplitude. Even though the flow is parallel and the stagnation area is considerably lower, increasing the amplitude still decreases the gas transfer. This decrease can be because increasing the amplitude increases the stagnation area, and since the flow is highly convective, it results in lower gas transfer.

6.1.2.2 Effect of Twist

Twisting the fiber introduces a helical structure that can create secondary flow patterns, enhancing fluid mixing around the fiber surface. This increased mixing can disrupt the boundary layer, reducing its thickness and potentially improving gas transfer rates. Sinusoidal fibers with an amplitude of 50 microns were twisted 0.5, 1, 1.5, and 2 turns. Figure 22 shows the O₂ partial pressure on the sinusoidal three twisted walls (flow moves from left to right):

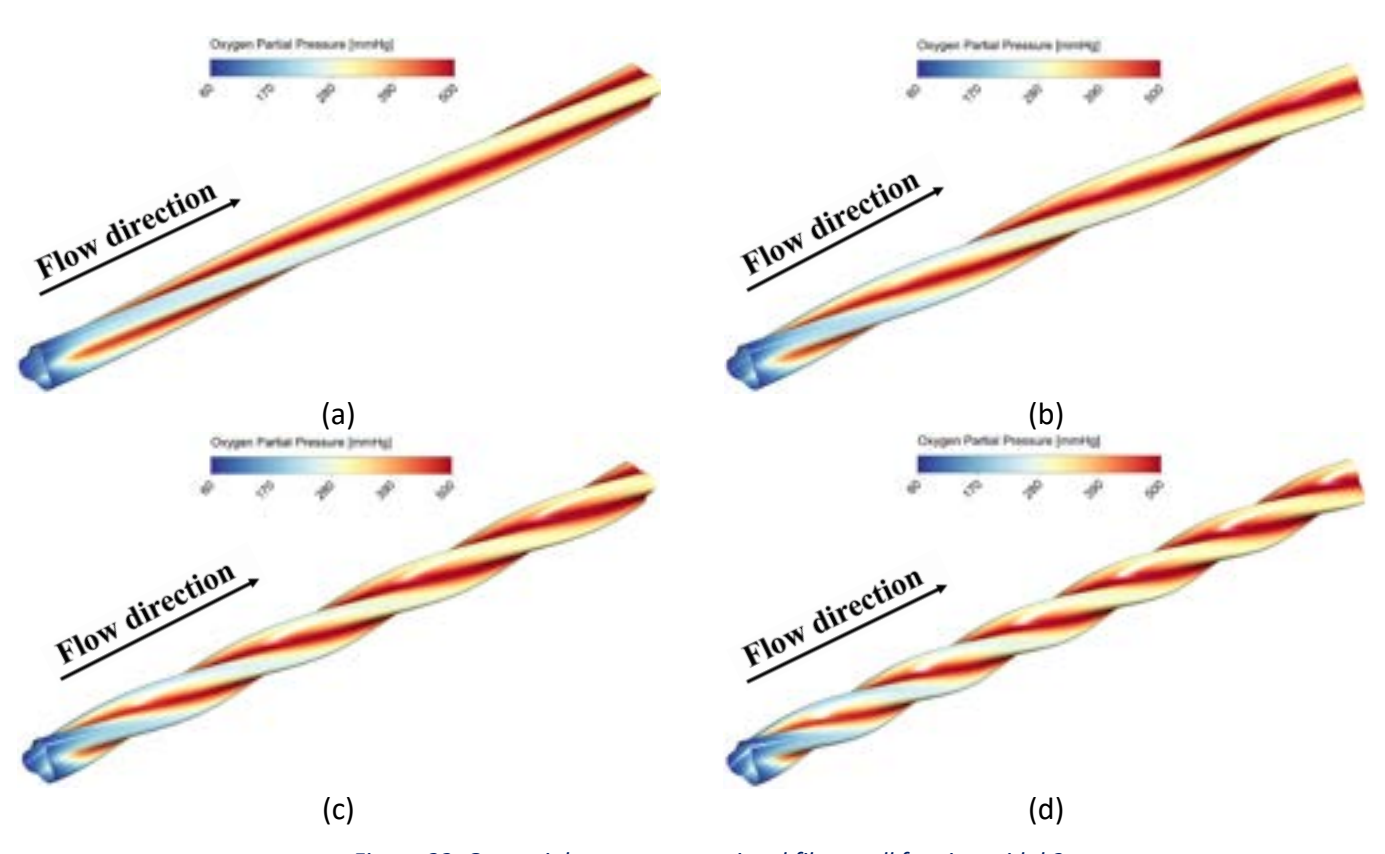


Figure 22. O₂ partial pressure on twisted fiber wall for sinusoidal 3

Figure 23 shows the effect of the number of turns on O_2 uptake and CO_2 removal. Increasing the number of turns decreases the O_2 uptake and CO_2 removal, But the difference is insignificant. For example, in sinusoidal 3, by increasing the number of turns from 0.5 to 2, the O_2 uptake decreases only by 0.9%. So, the effect of twisting the fiber on gas transfer can be neglected.

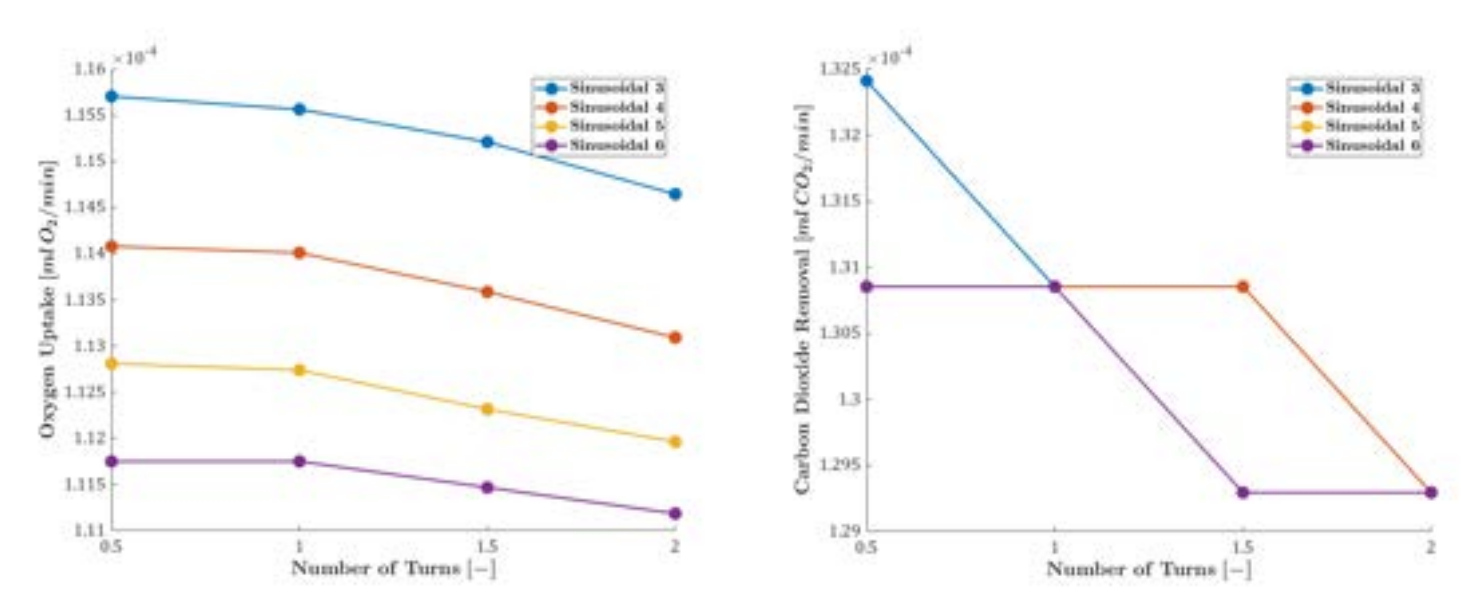


Figure 23. Effect of number of turns on O2 uptake and CO2 removal

Also, by evaluating the specific gas transfer, it can be confirmed that the effect of twisting the fiber is negligible on the gas transfer. Figure 24 shows the effect of the number of turns on specific O_2 uptake and specific CO_2 removal:

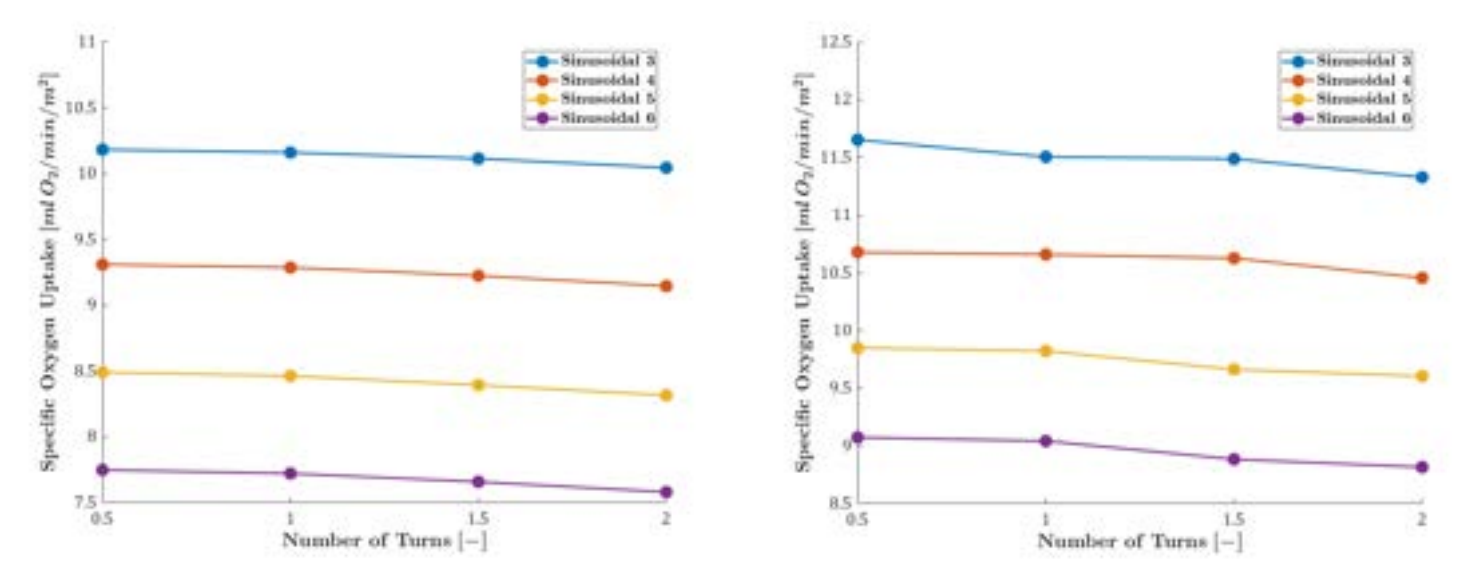


Figure 24. Effect of number of turns on specific O₂ uptake and specific CO₂ removal



6.2 Multi-fibers (20 Fibers)

Oxygen partial pressure contour at the midplane with cylindrical and sinusoidal fibers for the model with 20 fibers is shown in Figure 25:

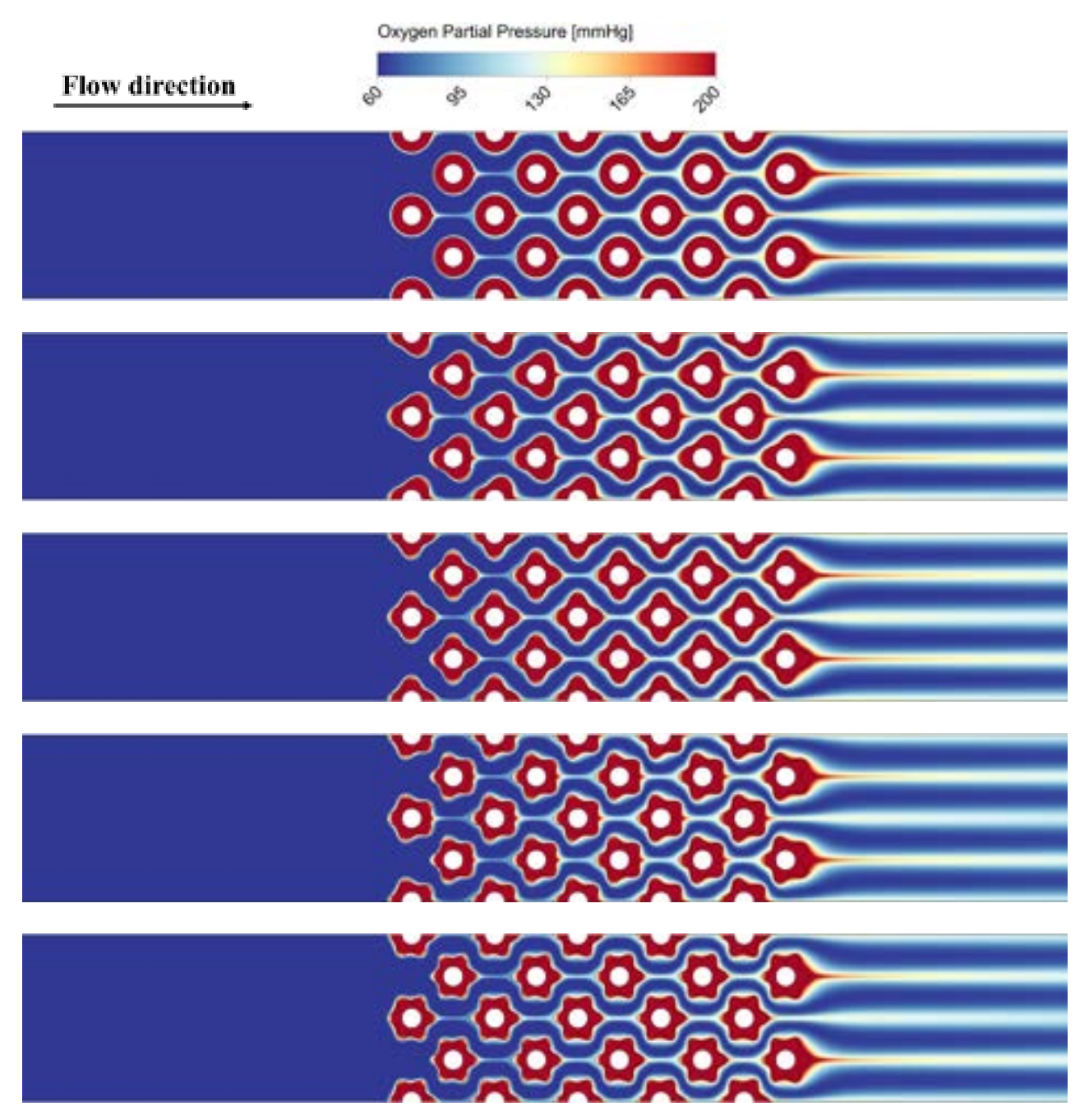
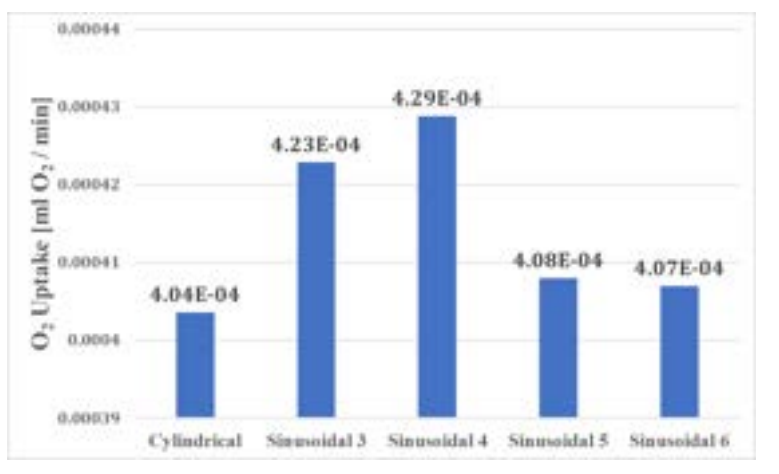


Figure 25. O₂ partial pressure for 20 fibers for different fibers

Considering multiple fibers, such as 20 fibers in a staggered position, is crucial for understanding the impact of fiber arrangement on flow dynamics and gas transfer efficiency. In real-world ECMO systems, blood interacts with an array of fibers, not just a single one, and the arrangement of these fibers affects the flow patterns, shear rates, and the distribution of oxygen and carbon dioxide. By analyzing the gas transfer across multiple fibers, we can better capture the interactions between

neighboring fibers, assess flow disturbances, and optimize fiber placement to enhance overall mass transfer performance in the oxygenator.

Figure 26 shows the O_2 uptake and CO_2 removal for the 20 fibers with different fiber shapes (amplitude of sinusoidal fibers is considered to be 50 microns):



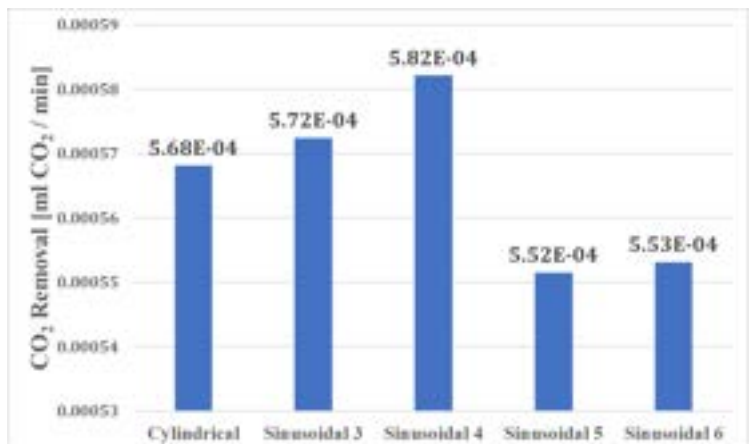
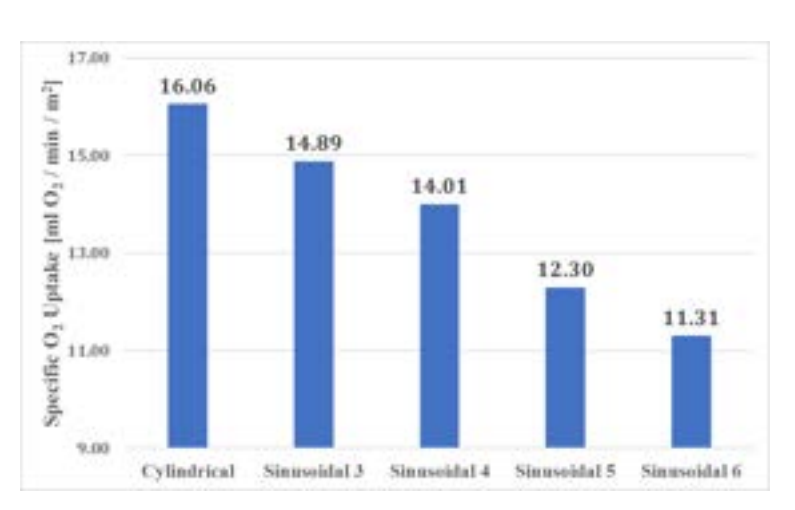


Figure 26. Gas transfer for 20 fibers with different fiber shapes

Figure 26 indicates that the gas transfer increases using sinusoidal 3 and sinusoidal 4. The maximum increase of gas transfer in comparison with cylindrical fiber, which happens with sinusoidal 4 fibers, is only 5.44% for O₂ uptake and 2.46% for CO₂ removal. Figure 27 shows the specific O₂ uptake and specific CO₂ removal. The specific gas transfer values show a similar behavior to a single fiber. Cylindrical fiber has the maximum specific gas transfer, and by using sinusoidal fibers, it decreases. By comparing Figure 27 and Figure 17, the specific gas transfer decreased for the 20 fibers model because by passing the flow over the fibers, the partial pressure increases, and by reducing the partial pressure difference, the gas transfer decreases.



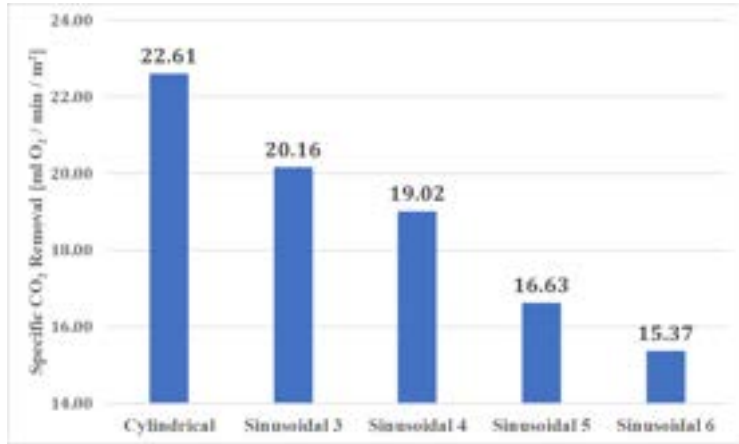


Figure 27. Specific gas transfer for 20 fibers with different fiber shapes



6.3 Multi-fibers (100 Fibers)

Oxygen partial pressure contour at the midplane with cylindrical and sinusoidal fibers for the model with 100 fibers is shown in Figure 28:

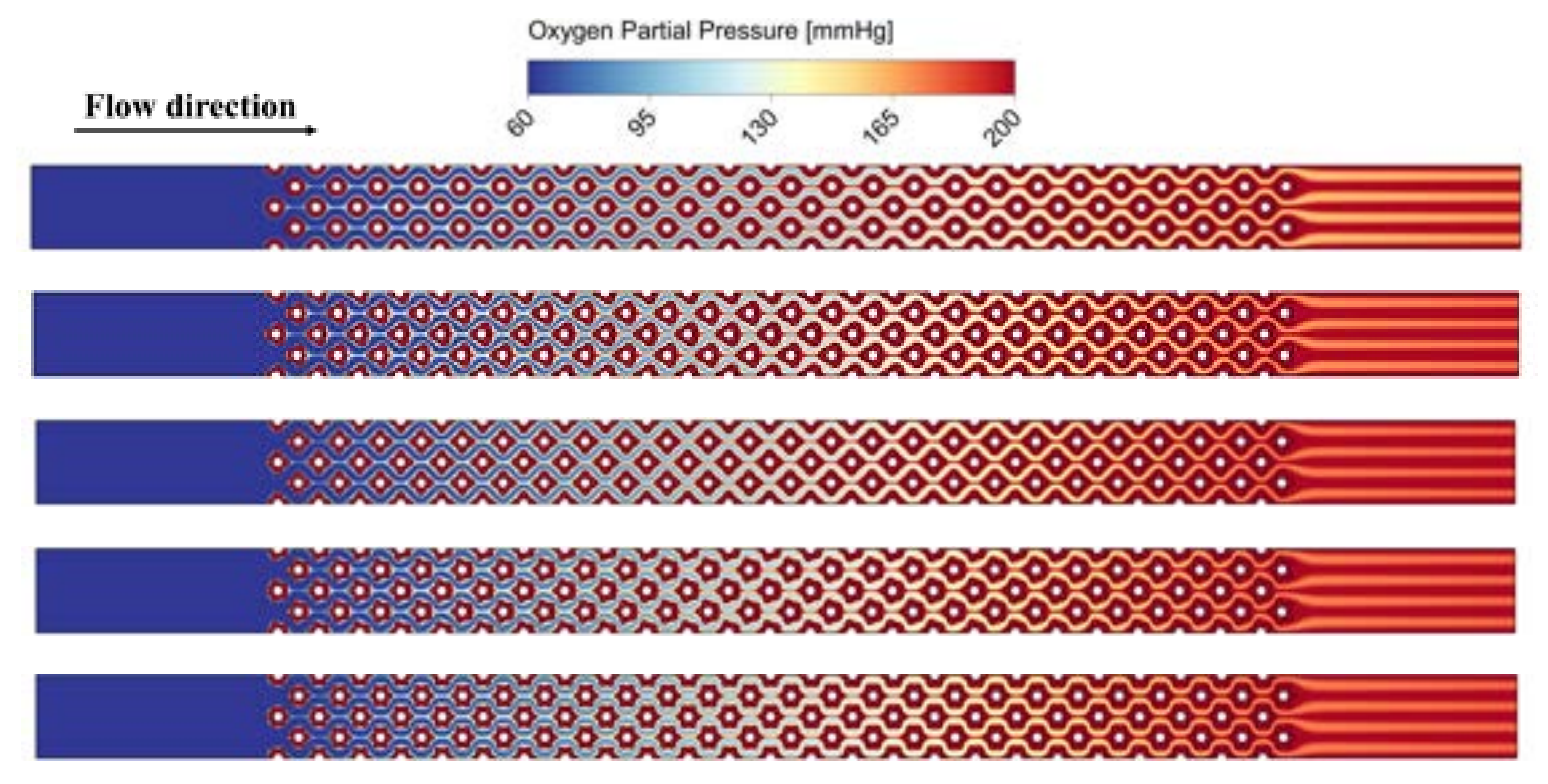


Figure 28. O₂ partial pressure for 20 fibers for different fibers

Figure 28 shows that using 100 fibers increases the gas transfer in sinusoidal fiber (more red area can be seen at the outlet of the sinusoidal fibers). Figure 29 shows the O_2 uptake and CO_2 removal value for the 100 fibers with different fiber shapes (the amplitude of sinusoidal fibers is considered to be 50 microns):

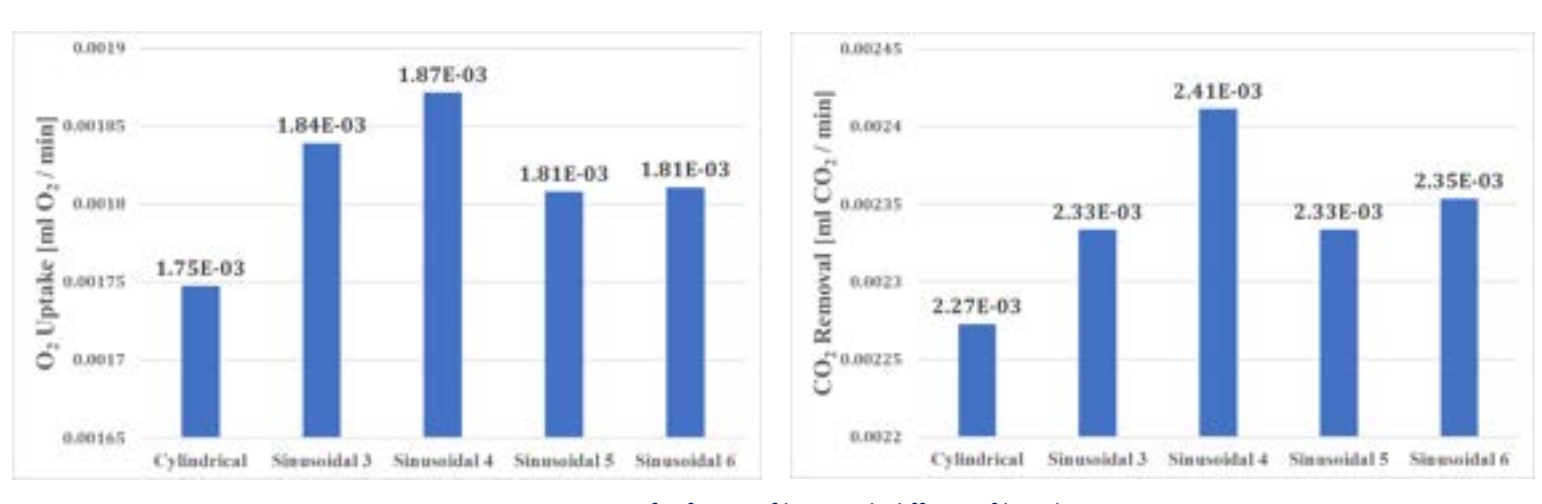


Figure 29. Gas transfer for 100 fibers with different fiber shapes

Figure 29 indicates that by using sinusoidal fibers, the gas transfer increases. The maximum increase of gas transfer compared with cylindrical fiber, which happens with sinusoidal 4 fibers, is only 6.85% for O_2 uptake and 6.16% for CO_2 removal. So, by using more fibers, the gas transfer shows a more reasonable value, O_2 uptake increases, and CO_2 removal decreases, the percentile gets closer. Also, this figure indicates that sinusoidal 4 and sinusoidal 3 are better regarding gas transfer.

Figure 30 shows the specific O₂ uptake and specific CO₂ removal. The specific gas transfer values show similar behavior to a single fiber in the model with 20 fibers. Still, the cylindrical fibers show higher specific gas transfer values in comparison with sinusoidal fibers. So, the specific gas transfer decreases even when the gas transfer is increased using sinusoidal fiber.

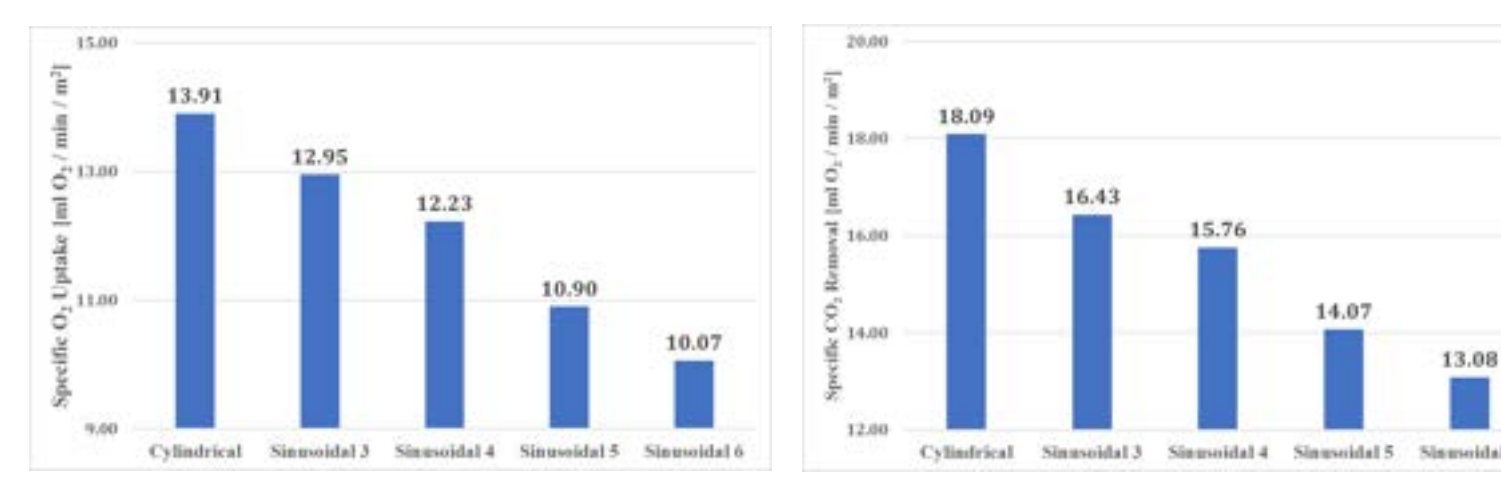


Figure 30. Specific gas transfer for 100 fibers with different fiber shapes

Although the specific gas transfer values are lower for sinusoidal fibers than cylindrical fibers, the overall total gas transfer increases when sinusoidal fibers are used. This suggests that optimizing the fibers' design and spatial arrangement within the oxygenator makes it possible to achieve higher total gas transfer and an improved gas transfer per unit volume of the oxygenator. Additionally, exploring alternative flow configurations, such as diagonal flow with an angle of attack, has the potential to enhance mass transfer by promoting more effective mixing and reducing stagnation zones. These strategies could significantly improve gas exchange efficiency in ECMO systems, making sinusoidal fibers a promising option for optimizing oxygenator performance.



7 CONCLUSIONS

This study provided a comprehensive O₂ and CO₂ transfer analysis in hollow fiber membranes, focusing on fiber geometries and flow configurations to optimize mass transfer performance. Through detailed CFD simulations, the effects of fiber shape, amplitude, and orientation on gas exchange efficiency were systematically evaluated for a single fiber under both transverse and parallel flow conditions. The results highlighted sinusoidal fibers with increased surface complexity can theoretically offer enhanced gas transfer due to a larger surface area. However, they also introduce flow disturbances that may negatively impact mass transfer rates, particularly at high Péclet numbers where convective transport dominates.

In the transverse flow configuration, increasing the amplitude of sinusoidal fibers decreased specific gas transfer rates, primarily due to the formation of thicker boundary layers and stagnation zones that hindered efficient gas exchange. Similarly, in the parallel flow configuration, the introduction of fiber twisting was found to have a negligible impact on gas transfer, indicating that while geometric modifications can alter flow dynamics, their effects on gas exchange are highly dependent on the balance between convective and diffusive transport mechanisms. With their streamlined geometry, the cylindrical fibers consistently showed better specific O₂ uptake and CO₂ removal, suggesting that in high Péclet number scenarios, simpler fiber geometries may be more effective.

The analysis of oxygen partial pressure and gas transfer across different fiber shapes and arrangements highlights the importance of considering fiber geometry and distribution in ECMO systems. For both the 20-fiber and 100-fiber models, sinusoidal fibers showed an increase in overall gas transfer efficiency compared to cylindrical fibers, with sinusoidal 4 fibers yielding the highest gains. In the 100-fiber model, the gas transfer increased by 6.85% for O₂ uptake and 6.16% for CO₂ removal, demonstrating that larger arrays of fibers enhance gas exchange. While sinusoidal fibers exhibit lower specific gas transfer values than cylindrical fibers, their overall total gas transfer is higher. This indicates sinusoidal fibers can enhance gas transfer efficiency with proper optimization of fiber design and arrangement, particularly when considering gas transfer per unit volume of the oxygenator. Additionally, alternative flow configurations, such as diagonal flow with an angle of attack, could further improve gas exchange by enhancing fluid mixing and reducing stagnation zones. These findings suggest that sinusoidal fibers offer a promising approach to improving the performance of ECMO systems and other blood oxygenators when combined with optimized flow patterns.

Overall, the study demonstrated the importance of considering fiber geometry and flow configuration when optimizing hollow fiber membranes for gas exchange applications. The findings suggest complex fiber shapes such as sinusoidal and twisted designs can influence flow behavior. However, their potential benefits in enhancing mass transfer must be carefully weighed against the induced flow disturbances. For high Péclet number flows, cylindrical fibers offer a more efficient gas transfer performance, emphasizing the need for a tailored approach in fiber design to achieve optimal outcomes in oxygenator applications.

8 REFERENCES

- [1] Liu H, Lan L, Abrigo J, Ip HL, Soo Y, Zheng D, Wong KS, Wang D, Shi L, Leung TW, Leng X. Comparison of Newtonian and non-Newtonian fluid models in blood flow simulation in patients with intracranial arterial stenosis. Frontiers in physiology. 2021 Sep 6;12:718540.
- [2] Sun H, Jiang Y, Zhang Y, Jiang L. A review of constitutive models for non-Newtonian fluids. Fractional Calculus and Applied Analysis. 2024 Jun 4:1-44.
- [3] Ecker P, Pekovits M, Yorov T, Haddadi B, Lukitsch B, Elenkov M, Janeczek C, Jordan C, Gfoehler M, Harasek M. Microstructured Hollow Fiber Membranes: Potential Fiber Shapes for Extracorporeal Membrane Oxygenators. Membranes. 2021 May 20;11(5):374.
- [4] Poletti G, Ninarello D, Pennati G. Computational Analysis of the Effects of Fiber Deformation on the Microstructure and Permeability of Blood Oxygenator Bundles. Annals of Biomedical Engineering. 2024 Apr;52(4):1091-105.
- [5] Badulak JH, Shinar Z. Extracorporeal membrane oxygenation in the emergency department. Emergency Medicine Clinics. 2020 Nov 1;38(4):945-59.
- [6] Taskin ME, Fraser KH, Zhang T, Griffith BP, Wu ZJ. Micro-scale modeling of flow and oxygen transfer in hollow-fiber membrane bundle. Journal of membrane science. 2010 Oct 15;362(1-2):172-83.
- [7] Eash HJ, Jones HM, Hattler BG, Federspiel WJ. Evaluation of plasma resistant hollow fiber membranes for artificial lungs. ASAIO journal. 2004 Sep 1;50(5):491-7.
- [8] Svitek RG, Federspiel WJ. A mathematical model to predict CO 2 removal in hollow fiber membrane oxygenators. Annals of biomedical engineering. 2008 Jun;36:992-1003.
- [9] Tang TQ, Hsu SY, Dahiya A, Soh CH, Lin KC. Numerical modeling of pulsatile blood flow through a mini-oxygenator in artificial lungs. Computer Methods and Programs in Biomedicine. 2021 Sep 1;208:106241.
- [10] International Civil Aviation Organization (ICAO). International Standard Atmosphere. ICAO Document 7488. 3rd ed. Montreal: ICAO; 1993.
- [11] Boyd J, Buick JM, Green S. Analysis of the Casson and Carreau-Yasuda non-Newtonian blood models in steady and oscillatory flows using the lattice Boltzmann method. Physics of Fluids. 2007 Sep 1;19(9).
- [12] Cussler EL. Diffusion: Mass Transfer in Fluid Systems. 2nd ed. Cambridge: Cambridge University Press; 1997. p. 122-123.



[13] Zhang J, Chen Z, Griffith BP, Wu ZJ. Computational characterization of flow and blood damage potential of the new maglev CH-VAD pump versus the HVAD and HeartMate II pumps. The International journal of artificial organs. 2020 Oct;43(10):653-62.

9 LIST OF FIGURES

Figure 1. CFD domain with boundaries and dimensions for a single fiber; a) Transverse flow, b) Parallel flow	9
Figure 2. CFD domain with boundaries and dimensions for 20 fibers	10
Figure 3. CFD domain with boundaries and dimensions for 100 fibers	10
Figure 4. Different non-Newtonian models for blood viscosity. a) Casson type models, b) Carreau type models, c)	
Power-law models	11
Figure 5. Planes to show the results, a) x-y midplane, b) x-z midplane	16
Figure 6. O2 partial pressure contour at x-y and x-z midplanes for scenario 1	16
Figure 7. O₂ partial pressure contour at x-y and x-z midplanes for scenario 2	17
Figure 8. O ₂ partial pressure contour at x-y and x-z midplanes for scenario 3	18
Figure 9. O₂ partial pressure contour at x-y and x-z midplanes for scenario 4	18
Figure 10. O₂ partial pressure contour at x-z midplane for scenario 44	19
Figure 11. The line for calculating O₂ partial pressure	21
Figure 12. O₂ partial pressure at the mentioned line for different cases and different meshes	22
Figure 13. 1500k elements mesh for sinusoidal 6 fiber with amplitude of 50 microns, a) full view, b) zoomed in	23
Figure 14. Generated mesh for fibers in a staggered position	23
Figure 15. O₂ uptake and CO₂ removal versus amplitude in the transverse flow configuration	25
Figure 16. Specific O₂ uptake and Specific CO₂ removal versus amplitude in the transverse flow configuration	
Figure 17. Specific gas transfer for different sinusoidal fibers with an amplitude of 50 microns in comparison with	
cylindrical fiber	26
Figure 18. Effect of rotation on O₂ uptake and CO₂ removal	27
Figure 19. Effect of rotation on specific O2 uptake and specific CO2 removal	28
Figure 20. Effect of amplitude on O₂ uptake and CO₂ removal in parallel flow	29
Figure 21. Effect of amplitude on specific O₂ uptake and specific CO₂ removal in parallel flow	29
Figure 22. O₂ partial pressure on twisted fiber wall for sinusoidal 3	30
Figure 23. Effect of number of turns on O2 uptake and CO2 removal	31
Figure 24. Effect of number of turns on specific O₂ uptake and specific CO₂ removal	31
Figure 25. O₂ partial pressure for 20 fibers for different fibers	32
Figure 26. Gas transfer for 20 fibers with different fiber shapes	33
Figure 27. Specific gas transfer for 20 fibers with different fiber shapes	33
Figure 28. O ₂ partial pressure for 20 fibers for different fibers	
Figure 29. Gas transfer for 100 fibers with different fiber shapes	34
Figure 30. Specific gas transfer for 100 fibers with different fiber shapes	35



10 LIST OF TABLES

Table 1. Fluid dynamic parameters used in this study	13
Table 2. Mass transfer results for cylindrical fiber in different scenarios	
Table 3. Mass transfer results for sinusoidal fiber with 3 waves in different scenarios	
Table 4. Mass transfer results for sinusoidal fiber with 6 waves in different scenarios	
Table 5. Root mean square error percentage of each mesh for different fibers	